AGU PUBLICATIONS

JGR

Journal of Geophysical Research: Earth Surface

RESEARCH ARTICLE
10.1002/2016JF003973

Key Points:
- Landscape evolution simulations reveal that channel profiles maintain quasi-equilibrium forms during active divide migration
- The timescale of channel response to drainage area change is predicted to be much less than the timescale of divide migration
- River profiles more strongly reflect spatiotemporal variation in rock uplift, climate, or rock properties than changes in drainage area

Supporting Information:
- Supporting Information S1
- Figure S1
- Figure S2
- Figure S3
- Figure S4
- Figure S5
- Figure S6
- Figure S7
- Movie S1
- Movie S2
- Movie S3

Correspondence to:
K. X. Whipple,
kxw@asu.edu

Citation:
Whipple, K. X., A. M. Forte, R. A. DiBiase, N. M. Gasparini, and W. B. Ouimet (2017), Timescales of landscape response to divide migration and drainage capture: Implications for the role of divide mobility in landscape evolution, *J. Geophys. Res. Earth Surf.*, *122*, doi:10.1002/2016JF003973.

Received 24 MAY 2016
Accepted 8 DEC 2016
Accepted article online 23 DEC 2016

Timescales of landscape response to divide migration and drainage capture: Implications for the role of divide mobility in landscape evolution

K. X. Whipple[1], A. M. Forte[1], R. A. DiBiase[2], N. M. Gasparini[3], and W. B. Ouimet[4]

[1]School of Earth and Space Exploration, Arizona State University, Tempe, Arizona, USA, [2]Department of Geosciences, Pennsylvania State University, University Park, Pennsylvania, USA, [3]Department of Earth and Environmental Sciences, Tulane University of Louisiana, New Orleans, Louisiana, USA, [4]Department of Geography and Center for Integrative Geosciences, University of Connecticut, Storrs, Connecticut, USA

Abstract Efforts to extract information about climate and tectonics from topography commonly assume that river networks are static. Drainage divides can migrate through time, however, and recent work has shown that divide mobility can potentially induce changes in river profiles comparable to changes caused by variation in rock uplift, climate, or rock properties. We use 1-D river profile and 2-D landscape evolution simulations to evaluate how mobile divides influence the interpretation of river profiles in tectonically active settings. We define a nondimensional divide migration number, N_{Dm}, as the ratio of the timescale of channel profile response to a change in drainage area (T_{dA}) to the timescale of divide migration (T_{Dm}). In simulations of headward divide migration, N_{Dm} is much less than unity with no measurable perturbation of channel profiles. Only in simulations configured to induce rapid lateral divide migration are there occasional large stream capture events and zones where localized drainage area loss is fast enough to support N_{Dm} values near unity. The rapid response of channel profiles to changes in drainage area ensures that under most conditions profiles maintain quasi-equilibrium forms and thus generally reflect spatiotemporal variation in rock uplift, climate, or rock properties even during active divide migration. This implies that channel profile form may not reliably record divide mobility, so we evaluate alternate metrics of divide mobility. In our simulations and an example in Taiwan, we find that simple measures of cross-divide contrasts in topography are more robust metrics of divide mobility than measures of drainage network topology.

1. Introduction

River incision is governed by water and sediment fluxes, and the importance of divide migration and drainage capture in long-term landscape evolution has long been recognized [e.g., *Gilbert*, 1877; *Davis*, 1903; *Glock*, 1931; *Bishop*, 1995]. Despite this, modern analyses of topography aimed at reconstructing spatiotemporal patterns of rock uplift rate or climatic conditions have generally either explicitly or implicitly assumed that divide mobility and drainage capture were at most minor complications. This conceptual framework was bolstered by a generation of landscape evolution models in which drainage networks quickly stabilize into invariant patterns unless strongly perturbed [*Tucker and Hancock*, 2010]. If divides are stable or slowly moving relative to the timescale of channel profile response, then the main challenges in the interpretation of river profile form stem from the need to quantify tectonic, climatic, and lithologic controls on river slope and to differentiate between spatial and temporal variations in these factors [e.g., see reviews by *Wobus et al.*, 2006; *Kirby and Whipple*, 2012; *Whittaker*, 2012; *Lague*, 2014]. Where rock properties and climate show minimal spatial variability, much work has contributed to developing insights into how spatial and temporal patterns of rock uplift rate will be manifest in landscape morphology, especially river profile forms [e.g., *Kirby and Whipple*, 2001, 2012; *Lavé and Avouac*, 2001; *Duvall et al.*, 2004; *Clark et al.*, 2005; *Craddock et al.*, 2007; *Harkins et al.*, 2007; *Whittaker et al.*, 2007; *Hilley and Arrowsmith*, 2008; *Cyr et al.*, 2010; *Attal et al.*, 2011; *Kirby and Ouimet*, 2011; *Miller et al.*, 2012; *Whittaker*, 2012; *Miller et al.*, 2013]. As they do not consider the potential for divide mobility, these studies essentially assume that large capture events are sufficiently rare and gradual divide migration sufficiently slow to allow river profiles to maintain equilibrium forms with respect to changes in drainage area —an untested hypothesis.

In recent years there has been increasing awareness that the potential for pervasive, persistent divide mobility is likely greater in nature than in early landscape evolution models [*Hasbargen and Paola*, 2000;

Clark et al., 2004; *Pelletier*, 2004; *Bonnet*, 2009; *Prince et al*., 2010, 2011; *Stark*, 2010; *Castelltort et al*., 2012]. Important new work has shown how river profiles may record changes in drainage area in ways that could greatly complicate efforts to interpret river profiles in terms of spatiotemporal patterns of rock uplift and climatic conditions [e.g., *Willett et al*., 2014; *Yang et al*., 2015]. The implications for interpretation of river profiles, however, are not yet fully resolved. *Willett et al*. [2014] argued conceptually that as a consequence of changing the distribution of drainage area in a watershed, mobile divides induce disequilibrium in bedrock river long profiles and thus decouple channel profiles from spatiotemporal patterns in climate, tectonics, and rock erodibility. The implicit assumption behind any study that suggests a dominant role of divide mobility is that river profile response to changes in drainage area is slow compared to rates of divide mobility and drainage reorganization. The fundamental challenge to established practices of topographic analysis and interpretation is that any river profile can be "read" either in terms of influences on channel slope (such as rock uplift rate, rock strength, bed cover, bed material grain size, and climatic conditions) or alternatively in terms of influences on upstream drainage area stemming from divide migration or stream capture. Both possibilities should be considered at all times, but what determines the conditions under which one or the other is dominant?

In this paper we tackle the underlying controls on the relative timescales of drainage area change and river profile response to that change. We restrict our analysis to tectonically active settings with spatially uniform rock erodibility and climate. We use the ratio of characteristic timescales to define two nondimensional numbers that quantitatively illuminate the degree to which drainage divide mobility is expressed in river profiles. We focus on this because only if the timescale of river profile response to drainage area change is short compared to the timescale of divide mobility can changes in drainage area be neglected in analyses of topography as is often assumed. Conversely, interpretation of river profiles primarily in terms of the direction and magnitude of drainage area change is only advisable if the timescale of river profile response is long compared to the timescale of divide mobility. Complementary to this analysis of relative timescales, we also assess the utility of potential metrics for determining the direction and rate of divide mobility.

2. Background

To frame our analysis, we begin with a review of the interrelationships among channel gradient, drainage area, drainage network topology, and erosion rates. We include a conceptual overview of how changes in drainage area resulting from divide migration influence the spatial pattern of river erosive power and thus the expected patterns of river profile evolution and the potential feedbacks with divide migration rates. In addition, we briefly review topographic metrics with potential to identify mobile divides and indicate the direction and/or rate of divide migration.

2.1. Metrics of River Profile Form and Relative Erosive Power

Many morphometric parameters commonly interpreted as proxies for local conditions (climate, rock properties, erosion rate, or rock uplift rate) can be influenced significantly by recent drainage area change. To frame an analysis of river profile response to divide migration, we begin with a brief review of morphometric parameters and analyses that are particularly useful for illuminating both the influence of divide migration and ensuing landscape response.

The channel steepness, k_{sn}, is essentially a metric of channel gradient corrected for differences in drainage area:

$$k_{sn} = SA^{\theta_{ref}}, \tag{1}$$

where S is local river gradient, defined as positive downstream, A is upstream drainage area, and θ_{ref} is a reference concavity index [*Wobus et al*., 2006]. Equation (1) makes it clear how a change in upstream drainage area (A) will instantly change k_{sn} before any erosional response can change the river profile. Furthermore, numerous empirical studies have shown robust, monotonic relationships between channel steepness and erosion rate E:

$$E = \alpha k_{sn}{}^{f}, \tag{2}$$

where α is expected to depend on rock properties and climate [e.g., *Ouimet et al*., 2009; *DiBiase et al*., 2010; *Kirby and Whipple*, 2012; *Godard et al*., 2014; *Lague*, 2014; *Scherler et al*., 2014] and the exponent f on the interaction of erosion thresholds and runoff variability [*Tucker*, 2004; *Lague et al*., 2005; *DiBiase and Whipple*, 2011]. These relationships among rock properties, climate, erosion rate, and channel steepness

underlie the interpretation of landscape evolution histories from analysis of river profiles. Thus, a change in k_{sn} caused by a change in upstream drainage area (equation (1)) is expected to change erosion rate and complicate interpretation of river profiles in terms of rock properties, climate, or tectonics.

Equation (1) forms the basis of both slope-area plots (S plotted as a function of A on logarithmic axes) and χ-transformed river profiles, developed in the so-called "integral method" of slope-area analysis [*Harkins et al*., 2007; *Perron and Royden*, 2012; *Mudd et al*., 2014]. The variable χ can be derived by solving equation (1) for S (river gradient) and integrating upstream (in x) from the outlet (x_b):

$$z = z_b + \left(k_{sn}/{A_0}^{\theta_{ref}}\right)\chi, \tag{3a}$$

where z is river bed elevation, z_b the elevation of the outlet of the catchment analyzed, and

$$\chi = \int_{x_b}^{x} \left(A_0/A\left(x'\right)\right)^{\theta_{ref}} dx', \tag{3b}$$

where x' is a dummy variable and A_0, the reference scaling area of *Perron and Royden* [2012], is best set to unity such that the slope of χ-transformed river profiles (z versus χ) is equal to the channel steepness (equation (3a)). Note that although the χ transformation is usually framed in the context of the detachment-limited stream power model, its utility is not tied to, nor limited by, any one river incision model.

Under steady state conditions with spatially uniform climate, lithology, bed characteristics, and rock uplift rate, χ-transformed river profiles are expected to be linear, with slope equal to the channel steepness, k_{sn}, so long as the choice of θ_{ref} appropriately characterizes river profile concavity (an incorrect choice of θ_{ref} will result in smoothly curving plots under these conditions) [*Harkins et al*., 2007; *Perron and Royden*, 2012; *Mudd et al*., 2014]. Both perturbations away from steady state and spatial variations in climate, rock strength, or rock uplift rate will manifest as spatial variations in k_{sn} [e.g., *Whittaker et al*., 2007; *Kirby and Whipple*, 2012; *Whittaker*, 2012; *Lague*, 2014] and thus curving or piecewise linear χ-transformed profiles, depending on the circumstances [e.g., *Perron and Royden*, 2012; *Mudd et al*., 2014].

2.2. River Profile Response to Drainage Area Change

Divide migration and associated drainage area change perturb river profiles and thus erosion rate patterns in ways that trigger both a positive, reinforcing feedback, and a negative, stabilizing feedback (Figure 1). As an aggressor stream gains area at the expense of a victim stream, the cross-divide erosion rate contrast between the aggressor and the victim tends to increase (equations (1) and (2)), driving faster divide migration and greater disequilibrium in channel profiles in a positive feedback loop, as emphasized by *Willett et al*. [2014]. However, a negative feedback acts in concert with this effect to reduce channel disequilibrium and thus inhibit the operation of the positive feedback (Figure 1). This occurs because, as detailed below, drainage area gains and losses also produce an imbalance between rock uplift rate, U, and erosion rate, E, that varies along stream in both the aggressor and victim catchments. This along-stream variation in the difference between U and E drives river profile adjustment toward equilibrium with local conditions (climate, rock properties, and rock uplift rate) and reduces cross-divide contrasts in erosion rates that drive divide migration [e.g., *Gilbert*, 1877]. Should the negative feedback dominate, river profiles would maintain quasi-equilibrium forms even in the presence of mobile divides. Therefore, our analysis is directed at resolving the conditions under which the positive or negative feedback mechanisms may control landscape response to divide migration.

Analogous to the influence of spatiotemporal variability in rock uplift rate, rock properties, or river erosivity (climate), *Willett et al*. [2014] demonstrated how changes in drainage area can produce similar, smoothly curving, perturbations to the shape of χ-transformed profiles and thus spatial distributions of k_{sn} (the local slope of χ-transformed profiles) downstream of the gain or loss of drainage area (Figure 2a). A change to upstream drainage area immediately changes χ:χ decreases with area gain and increases with area loss proportional to the fractional change in area, with no change to river bed elevation or gradient. The increase in k_{sn} following area gain and decrease in k_{sn} following area loss is visually apparent as changes in the slope of χ-transformed profiles (Figure 2a). A given change in area has a greater influence at small drainage areas, resulting in curving χ-transformed river profiles downstream of the point of area change. Thus, paired concave-up (area gain) and convex-up (area loss) χ-transformed river profiles on either side of a divide would be clearly diagnostic of recent divide migration or capture [*Willett et al*., 2014].

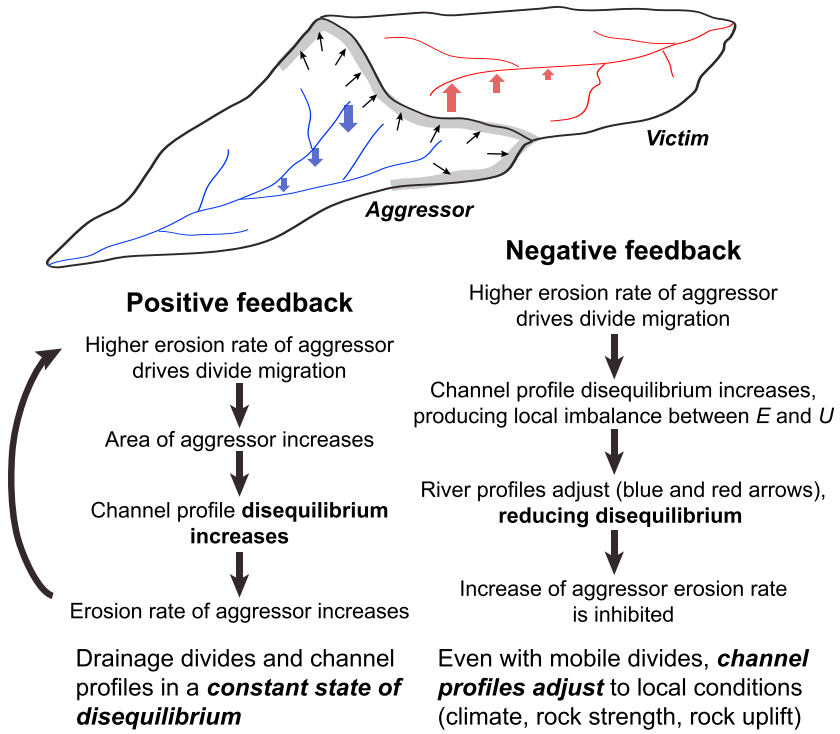

Figure 1. Conceptual illustration of competing positive and negative feedbacks in divide migration. The positive feedback mechanism is well described by *Willett et al*. [2014]. The negative feedback mechanism in which river profile response to local imbalance between erosion, *E*, and rock uplift, *U*, acts to restore equilibrium. This prevents the development of a runaway condition of ever greater profile disequilibrium and ever greater divide migration rates expected if the positive feedback were left unchecked. The degree to which channel profiles record evidence of divide mobility depends on the relative timescales of divide migration and river profile adjustment.

The positive feedback mechanism described by *Willett et al*. [2014] is highlighted in Figures 1 and 2a and explained with the heavy blue (aggressor) and red (victim) lines in Figure 2c. Figure 2a illustrates that where channel profile erosional response is negligible on the timescale of divide migration, the disequilibrium of river profiles (deviation from the black line, representing a steady state profile with uniform $E = U$) steadily increases with progressive divide migration. The final state shown in Figure 2a (40% change in area) is used to illustrate the positive feedback in Figure 2c. Area gain leads to an increase in profile disequilibrium that increases headwater k_{sn} (slope of χ-transformed profile, Figure 2a) which in turn leads to an increase in erosion rate (equation (2)) commensurate with area gain (Figure 2c, heavy blue line). Similarly, the decrease in headwater k_{sn} with area loss leads to a commensurate decrease in erosion rate (Figure 2c, heavy red line). This increase in erosion rate in the headwaters of the aggressor catchment paired with a decrease in erosion rate in the headwaters of the victim catchment increases the cross-divide erosion rate contrast and thus increases the rate of divide migration, which in turn increases profile disequilibrium and reinforces the cross-divide erosion rate contrast. In landscapes where this positive feedback mechanism is a dominating influence, channel profiles would persist in a disequilibrium state, preserving an interpretable record of divide migration as argued by *Willett et al*. [2014].

The closely related negative feedback mechanism introduced here and described above is explained in the patterns of river profile evolution illustrated by the black and grey arrows in Figures 2b and 2c. As noted above, erosion rates will increase in a channel which gains area (the χ-transformed profile steepens, and thus, k_{sn} increases, which increases *E*; see equation (2)), such that an imbalance between rock uplift and erosion ($E > U$) results, leading to lowering of the river bed. Similarly, a channel that loses area will experience $E < U$ in its headwaters, resulting in net uplift of the river bed. Importantly, the degree of disequilibrium is nonuniform and increases toward the divide (Figure 2). As a result of the nonuniform imbalance between *E* and *U*, channel profiles adjust to restore equilibrium (black and grey arrows and timelines in Figures 2b

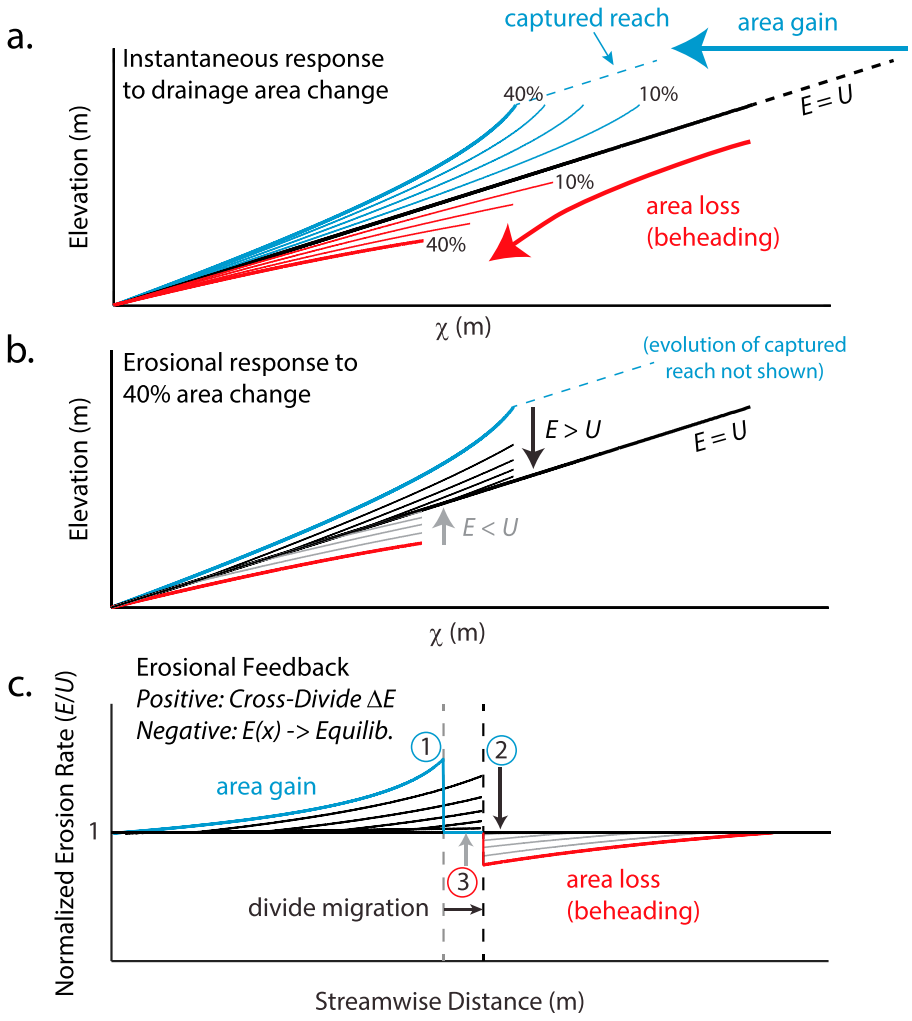

Figure 2. Schematic illustration of river profile response to drainage area change. (a) Instantaneous response to area change with no erosion. Initial condition (black line) is a steady state profile (erosion balancing rock uplift, $E = U$) with uniform channel steepness, k_{sn}, that includes a segment about to be captured (dashed). Area gain or loss instantaneously changes χ but not river bed elevation, decreasing χ for area gain (blue lines) and increasing χ for area loss (red lines). If erosional response is negligible compared to the timescale of divide migration, intermediate curves represent time steps as area change increases from 10 to 40% of initial area. Greater fractional changes in χ where drainage area is small result in curving χ-transformed profiles and thus nonuniform k_{sn} values. Captured reach experiences a uniform decrease in χ (dashed blue). In the case of area loss, for a beheaded catchment both maximum elevation and maximum χ are reduced by truncation. (b) Erosional response to area change. Immediately after the change in drainage area, the change to nonuniform k_{sn} initiates differential erosion patterns and a return toward the initial steady state form (black and grey arrows and time lines). The increased incision rate at the capture point on the aggressor channel will trigger a wave of incision that will migrate upstream into the captured reach (not shown). (c) Erosional feedback mechanisms. The response to area change creates a cross-divide erosion rate contrast (points 1 versus 3 or 2 versus 3 after incision wave reaches the new divide) that will enhance the rate of divide migration and amplify the distortion of χ-transformed profiles (Figure 2a)—the positive feedback described by *Willett et al.* [2014]. However, the response to differential erosion patterns shown in Figure 2b acts to rapidly diminish the cross-divide erosion rate contrast (black and grey arrows and timelines as in Figure 2b) and thus erase the morphological signature of divide migration—a negative feedback.

and 2c), resulting in a negative feedback—both the degree of profile disequilibrium and cross-divide erosion rate contrasts are reduced. Recent studies of natural examples suggest that the river profile response is quite rapid [*Brocard et al.*, 2012; *Yanites et al.*, 2013]. We hypothesize that the negative feedback ultimately controls the establishment of statistically stable drainage divide positions and works to equilibrate channel profile forms even during active divide migration.

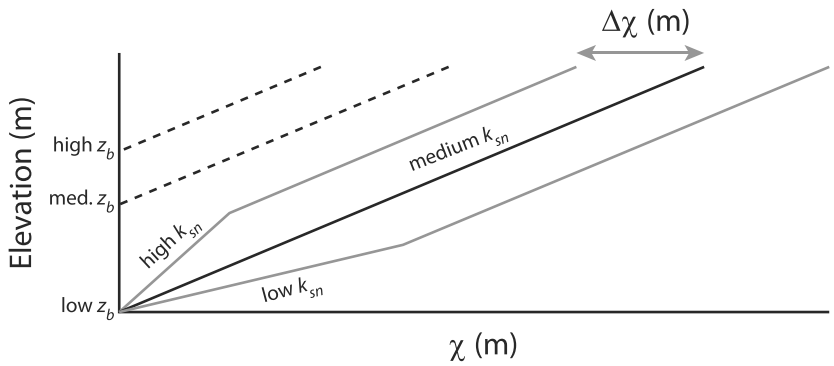

Figure 3. Illustration of χ anomalies ($\Delta\chi$) with stable divides. Only for spatially and temporally uniform channel steepness, k_{sn} (and thus spatially uniform rock uplift rate, U, and erosional efficiency, K) and uniform catchment outlet elevations, z_b, are no cross-divide differences in χ expected (all river profiles collapse onto the solid black line [e.g., *Perron and Royden*, 2012]. However, at steady state with stable divides any spatial variation in past or present U or K within the study site will manifest as differences in k_{sn} (slope of χ-transformed river profiles) and result in cross-divide differences in χ (solid grey lines). Differences in outlet elevation (z_b) will likewise create χ anomalies despite stable divide positions whether variation in z_b reflects differences in baselevel or simply choice of outlet location for analysis (dashed lines).

During divide migration there is thus a continuous competition between perturbation of channel profiles caused by changing upstream drainage area and the erosional response that acts to restore channel profiles to equilibrium forms (Figure 2). Ultimately, the tendency for differential erosion to restore equilibrium profile forms must prevail as divides migrate to equilibrium positions as envisioned in *Gilbert's* [1877] law of divides, but an important open question is whether, and under what conditions, diagnostic patterns of profile disequilibrium persist during active divide migration.

2.3. Metrics of Divide Mobility

Across-divide differences in χ (termed a "χ anomaly") have been proposed as an indicator of potential divide instability, and at least in one case in the Appalachian Mountains χ anomalies were shown to be proportional to cross divide differences in erosion rate and thus to divide migration rate [*Willett et al*., 2014]. As pointed out by *Willett et al*. [2014], however, χ anomalies can arise for many reasons. Indeed, any spatial variability in rock uplift rate, rock properties, or climate that influence channel steepness will manifest as significant χ anomalies even if divides are stable (Figure 3). Thus, in the presence of spatial variability in rock uplift rate, rock properties, or climate, χ anomalies cannot be expected to accurately indicate whether divides are mobile or potentially mobile, the direction of divide mobility, or the rate of divide migration. Moreover, a simple intercatchment difference in outlet elevation, z_b, will cause a significant χ anomaly (dashed lines, Figure 3). Note that a difference in outlet elevation could be related to real differences in baselevel or may simply be determined by the position of outlets chosen for analysis. Given these potential complications, we present and evaluate alternative metrics of divide mobility (both migration direction and migration rate) less dependent on assumptions and more directly related to the cross-divide differences in erosion rate required to actually drive divide migration as described in *Gilbert's* [1877] law of unequal slopes: cross-divide differences in channel elevation at a reference drainage area, mean headwater hillslope gradient, and mean headwater local relief. Differences in channel steepness, k_{sn}, may also be effective at the scale of second- or third-order basins but often cannot be measured in the immediate vicinity of the divide, and so we do not focus on cross-divide differences in k_{sn} here.

3. Approach and Scope

We focus primarily on theoretical considerations, building on the work of *Willett et al*. [2014] by further developing the understanding of the response of landscapes governed by the simple detachment-limited stream power family of models [*Howard*, 1994; *Whipple and Tucker*, 1999]:

$$E = KA^m S^n, \tag{4}$$

Table 1. Parameters and Key Results for FastScape Simulations

K (yr^{-1} for $n=1$; $m^{-1}\,yr^{-1}$ for $n=2$)	U_{max} ($m\,yr^{-1}$)	U_{min} ($m\,yr^{-1}$)	n	T_{Dm} (year) tilt	T_{Dm} (year) return[a]	D_{mr_max} ($m\,yr^{-1}$)
Runs Varying Erosional Efficiency (K)						
1.0×10^{-6}	1.0×10^{-3}	1.0×10^{-4}	1	1.25×10^{8}	1.46×10^{8}	1.93×10^{-5}
5.0×10^{-6}	1.0×10^{-3}	1.0×10^{-4}	1	2.33×10^{7}	2.48×10^{7}	9.57×10^{-5}
1.0×10^{-5}	1.0×10^{-3}	1.0×10^{-4}	1	1.41×10^{7}	2.24×10^{7}	1.89×10^{-4}
5.0×10^{-5}	1.0×10^{-3}	1.0×10^{-4}	1	2.34×10^{6}	2.03×10^{6}	9.58×10^{-4}
1.0×10^{-4}	1.0×10^{-3}	1.0×10^{-4}	1	8.62×10^{5}	1.12×10^{6}	1.86×10^{-3}
1.0×10^{-8}	5.0×10^{-3}	5.0×10^{-6}	2	9.60×10^{6}		1.00×10^{-4}
1.0×10^{-7}	5.0×10^{-3}	5.0×10^{-6}	2	3.56×10^{6}		3.66×10^{-4}
1.0×10^{-6}	5.0×10^{-3}	5.0×10^{-6}	2	1.29×10^{6}		1.12×10^{-3}
1.0×10^{-5}	5.0×10^{-3}	5.0×10^{-6}	2	3.32×10^{5}		1.89×10^{-3}
Runs Varying Uplift Rate (U_{max}, U_{min})[b]						
1.0×10^{-5}	5.0×10^{-4}	5.0×10^{-5}	1	1.46×10^{7}	1.87×10^{7}	1.77×10^{-4}
1.0×10^{-5}	1.0×10^{-3}	1.0×10^{-4}	1	1.41×10^{7}	2.24×10^{7}	1.89×10^{-4}
1.0×10^{-5}	2.0×10^{-3}	2.0×10^{-4}	1	1.39×10^{7}	2.11×10^{7}	1.86×10^{-4}
1.0×10^{-5}	3.0×10^{-3}	3.0×10^{-4}	1	1.36×10^{7}	1.86×10^{7}	1.96×10^{-4}
1.0×10^{-5}	4.0×10^{-3}	4.0×10^{-4}	1	1.45×10^{7}	1.73×10^{7}	1.94×10^{-4}
1.0×10^{-5}	8.0×10^{-3}	8.0×10^{-4}	1	1.18×10^{7}	1.67×10^{7}	1.89×10^{-4}
1.0×10^{-5}	1.2×10^{-2}	1.2×10^{-3}	1	1.32×10^{7}	1.73×10^{7}	1.98×10^{-4}
1.0×10^{-5}	2.0×10^{-2}	2.0×10^{-3}	1	1.35×10^{7}	2.10×10^{7}	1.80×10^{-4}
1.0×10^{-5}	5.0×10^{-2}	5.0×10^{-3}	1	1.27×10^{7}	1.64×10^{7}	1.88×10^{-4}
1.0×10^{-7}	5.0×10^{-4}	5.0×10^{-7}	2	8.69×10^{6}		1.00×10^{-4}
1.0×10^{-7}	2.5×10^{-3}	2.5×10^{-6}	2	4.96×10^{6}		2.26×10^{-4}
1.0×10^{-7}	4.0×10^{-3}	4.0×10^{-6}	2	5.09×10^{6}		3.06×10^{-4}
1.0×10^{-7}	5.0×10^{-3}	5.0×10^{-6}	2	3.36×10^{6}		3.58×10^{-4}
1.0×10^{-7}	6.0×10^{-3}	6.0×10^{-6}	2	3.81×10^{6}		4.08×10^{-4}
1.0×10^{-7}	7.5×10^{-3}	7.5×10^{-6}	2	2.65×10^{6}		4.28×10^{-4}
1.0×10^{-7}	1.0×10^{-2}	1.0×10^{-5}	2	2.69×10^{6}		4.27×10^{-4}

[a] For $n=2$ only the tilting phase was simulated.
[b] U_{max}/U_{min} ratio held constant for each value of n.

where K is the erosional efficiency (a function of rock properties and climate), and for which the reference concavity index is set by the m/n ratio ($\theta_{ref}=m/n$), typically near 0.5 [*Tucker and Whipple*, 2002; *Whipple et al*., 2013]. At steady state ($E=U$), local channel steepness is given by

$$k_{sn} = (U/K)^{1/n}, \tag{5}$$

consistent with observations represented in equations (1) and (2). Solving equation (5) for U (equal to E at steady state) shows that for the stream power model, α and f in equation (2) are K and n, respectively. In all cases we hold $m/n=0.5$. Although we use $n=1$ in several of the examples shown in figures, our analysis of timescales of landscape response is general and applicable to all values of the slope exponent n, as illustrated with comparable simulations with $n=2$ (Table 1 and the supporting information). The detachment-limited stream power river incision model additionally has well-known limitations [e.g., *Sklar and Dietrich*, 2004; *Whipple et al*., 2013; *Lague*, 2014]. Although formulated in terms of the stream power model, our results are readily extended to, and consistent with, any river incision model that predicts a systematic relationship between erosion rate and channel steepness consistent with equation (2), both at steady state and during periods of adjustment. We discuss only briefly the complications that likely arise in most natural landscapes (where deviations from predictions of equation (2), and thus equation (4), can be expected) and how they may manifest in divide mobility and metrics developed to assess the direction and speed of divide migration. We use a combination of 1-D channel profile models and 2-D landscape evolution models to test, illustrate, and quantify theoretical expectations for the relative timescales of divide migration and channel profile response to drainage area change, following earlier work by *Whipple and Tucker* [1999] and *Whipple* [2001].

To provide a simple quantitative framework for evaluating the relative influence of divide mobility on channel profile forms, we define two nondimensional numbers from the ratios of relevant timescales. The two relevant timescales are (1) the timescale over which channel profiles equilibrate following a perturbation caused by drainage area gain or loss, T_{dA}, and (2) the timescale of divide migration, T_{Dm}, defined as the

duration of divide migration to a new equilibrium position following a tectonic or climatic perturbation, such as that illustrated in the simulation presented by *Willett et al*. [2014]. The divide migration timescale is thus inversely related to the average rate of divide migration which sets the rate of drainage area gain or loss. Although the dynamic response of channel profiles and the resulting patterns of erosion are an essential part of the divide migration process, the degree to which progressive, gradual divide migration can be expected to influence river profile form (Figure 2) is governed by the ratio of these two timescales, defined here as the divide migration number, N_{Dm}:

$$N_{\mathrm{Dm}} = T_{\mathrm{d}A}/T_{\mathrm{Dm}}. \tag{6}$$

We propose that in the future the divide migration number be named the Gilbert divide migration number, given the close relation between our analysis and Gilbert's law of divides and associated law of unequal slopes which explains how divide migration is driven by cross-divide differences in erosion rate [*Gilbert*, 1877]. For $N_{\mathrm{Dm}} > 1$, erosional response of the channel to drainage area change is slower than the divide migration rate, causing significant perturbation of χ-transformed channel profiles (Figure 2a). As drainage area can also change via occasional large river capture events, we also define the drainage capture number, N_c, as the ratio of $T_{\mathrm{d}A}$ to the characteristic recurrence interval of large capture events (>5% change in precapture drainage area), T_c:

$$N_c = T_{\mathrm{d}A}/T_c. \tag{7}$$

For $N_c > 1$, large drainage capture events recur before channels can respond to prior capture events, and perturbed channel profiles can be expected to be relatively common.

Combining theory with 1-D channel profile models, we determine the controls on the timescale of channel profile response to either an instantaneous increase or decrease in drainage area by stream capture, $T_{\mathrm{d}A}$. In addition, by varying the timescale over which a drainage area change is imposed in 1-D profile evolution simulations, we illustrate the utility of the divide migration number, N_{Dm}, for scenarios involving gradual divide migration. We then use 2-D landscape evolution model (FastScape) [*Braun and Willett*, 2013] simulations to (1) test expectations for the controls on the timescale of headward divide migration (T_{Dm}) triggered by a tectonic (or climatic) perturbation and (2) evaluate landscape response under conditions where significant stream capture events are common. Finally, we develop and test a set of alternative metrics of divide instability, along with the χ-anomaly metric proposed by *Willett et al*. [2014], using our simulated landscapes. We discuss the implications of our findings both in general and with respect to a natural example of a landscape with previously identified mobile divides in the Central Range of Taiwan.

4. Analysis of Landscape Response

4.1. Timescale of Channel Profile Response to an Instantaneous Drainage Area Change by Stream Capture

Under the assumption of fixed divides, *Whipple* [2001] showed that the timescales $T_{\mathrm{d}U}$ and $T_{\mathrm{d}K}$ of channel profile response to a sudden fractional change in either rock uplift rate ($f_U = U_f/U_i$) or erosional efficiency ($f_K = K_f/K_i$) (where the subscripts i and f denote initial and final values), respectively, are given by

$$T_{\mathrm{d}U} = \beta K^{-1/n} U^{(1/n-1)} G(f_U) \tag{8a}$$

and

$$T_{\mathrm{d}K} = \beta K^{-1/n} U^{(1/n-1)} G(f_K), \tag{8b}$$

where K and U are the initial values of these variables in cases where they change (i.e., U in $T_{\mathrm{d}U}$ and K in $T_{\mathrm{d}K}$). β is a geometric factor (constant for immobile divides) given by

$$\beta = k_a^{-m/n} (1 - hm/n)^{-1} \left(L^{(1-hm/n)} - x_c^{(1-hm/n)} \right), \tag{9}$$

where the relationship between upstream drainage area (A) and streamwise distance downstream (x_d) is dictated by Hack's law [*Hack*, 1957], $A = k_a x_d^h$, where k_a and h are empirical constants, x_c is distance from divide to channel head, and L is streamwise distance from divide to outlet [*Whipple and Tucker*, 1999]. The function G depends on f_U for a change in uplift rate (reducing to $G = 1$ for $n = 1$) and depends on f_K for a change in erosional efficiency (change in climate, sediment load, or strength of exposed rock) but retains a dependence on f_K for $n = 1$ [*Whipple*, 2001]. Note that for $n = 1$, the timescale of channel profile response to a change in tectonics reduces to $T_{\mathrm{d}U} = \beta/K$, independent of both the initial uplift rate and the magnitude of change.

A sudden change in drainage area can be expected to induce a response similar to a change in climate as both involve a change in river discharge. Thus, we hypothesize that the timescale T_{dA} of river profile response to sudden fractional percent change in drainage area, f_A, should take the form

$$T_{dA} = \beta K^{-1/n} U^{(1/n-1)} G(f_A), \tag{10}$$

implying that there will be no dependence on U for $n = 1$ and that response time will decrease with increasing rock uplift rate for $n > 1$. We define f_A as the absolute value of the fractional percent change in watershed area ($f_A = |(A_f/A_i - 1)|$). Note that this definition of f_A means that, for example, both a 40% increase in area and a 40% decrease in area result in the same value of f_A. This choice reflects the fact that $G(f_A)$ is not dependent on the direction of area change, as we show below. We take β as the initial steady state value and note that both river length and basin shape will evolve during divide migration. $G(f_A)$ is unknown and defined to encompass any change in β from the initial state but is discoverable via numerical simulations. Analogous to $G(f_K)$ in equation (8b) [*Whipple*, 2001], $G(f_A)$ likely will not reduce to unity even for $n = 1$. The hypothesized form of equation (10) is thus semiempirical but the value of $G(f_A)$ is readily determined from numerical simulations.

We ran a series of 1-D channel profile evolution models (forward-space, forward-time finite difference solution scheme) for a wide range of initial river length ($10\,\text{km} \le L \le 100\,\text{km}$), uniform erosional efficiency ($10^{-7}\,\text{yr}^{-1} \le K \le 10^{-5}\,\text{yr}^{-1}$), uniform rock uplift rate ($0.1\,\text{mm/yr} \le U \le 5\,\text{mm/yr}$), slope exponent ($1/2 \le n \le 2$), and fractional change in area ($0.02 \le f_A \le 0.40$), including both area gain and area loss, to test the form of equation (10) and to empirically determine $G(f_A)$ (Figures 4 and S1). Given an asymptotic approach to steady state, we computed response time T_{dA} as the time required for erosion rates everywhere along the channel to reach within 1% of the steady state value ($E = U$). We find that predictions of equation (10) match model results very well and that the timescale of response is the same for area gain and area loss (Figure 4d) but depends on n and the magnitude of drainage area change approximately following (Figure S1)

$$G(f_A) = 0.68\frac{1 - f_A}{n}. \tag{11}$$

Importantly, $G(f_A)$ is independent of K and U. Although an analytical solution to discover a more rational form for $G(f_A)$ would be preferable, our analysis confirms that equation (10) captures the dependence of channel response time to an abrupt change in drainage area and that for $n = 1$, $T_{dA} = \beta\, G(f_A)/K$, with no dependence on U. In comparison, for $n = 2$, T_{dA} scales inversely with the square root of both K and U: $T_{dA} = \beta\, G(f_A)/(KU)^{0.5}$. For the full range of conditions tested, $G(f_A)$ varies between 0.2 and 1.2 and between 0.4 and 0.8 for cases with $n = 1$. Thus, for $n = 1$, the timescale of channel profile response to sudden drainage area change depends primarily on rock strength and the erosivity of the climate, K (Figure 4d), and is 40%–80% of the timescale of channel profile response to a change in rock uplift rate assuming fixed divides (equation (8a)). The rapid adjustment of river profiles following a change in drainage area seen in our models is consistent with recent studies that have evaluated the timescales involved in natural examples [*Brocard et al.*, 2012; *Yanites et al.*, 2013].

4.2. Timescales and Patterns of Landscape Response to Progressive Divide Migration

The influence of gradual divide migration on channel profiles depends critically on the rate of divide migration relative to the channel profile response time determined above, as reflected in N_{Dm} (equation (6)). To illustrate how N_{Dm} controls the degree of disequilibrium that develops in channel profiles during periods of active divide migration, we ran a suite of 1-D profile evolution simulations (analogous to those in Figure 4) in which drainage area is added at a constant, imposed rate at the head of an initially steady state river profile with uniform channel steepness. All simulations are identical except for imposed differences in the divide migration rate and, thus, the rate of drainage area gain. The effect of the divide migration number on χ-transformed river profiles is shown in Figure 5 for a 50% increase in drainage area and values of N_{Dm} ranging from 0.2 to infinity (the case of instantaneous drainage area change). A complementary supplemental figure shows several intermediate time steps during profile evolution for each case (Figure S2). N_{Dm} exerts a clear control on the degree of profile disequilibrium during active divide migration. For $N_{Dm} \ge 10$, erosional response is negligible relative to the rate of drainage area gain, and a clear, interpretable signature of divide migration is recorded in channel profiles. Conversely, for $N_{Dm} \le 0.5$ channel profiles maintain quasi steady state forms during active divide migration because erosional response keeps pace with gains in drainage area; the negative feedback is dominant, and there is no discernable record of divide migration in channel profiles.

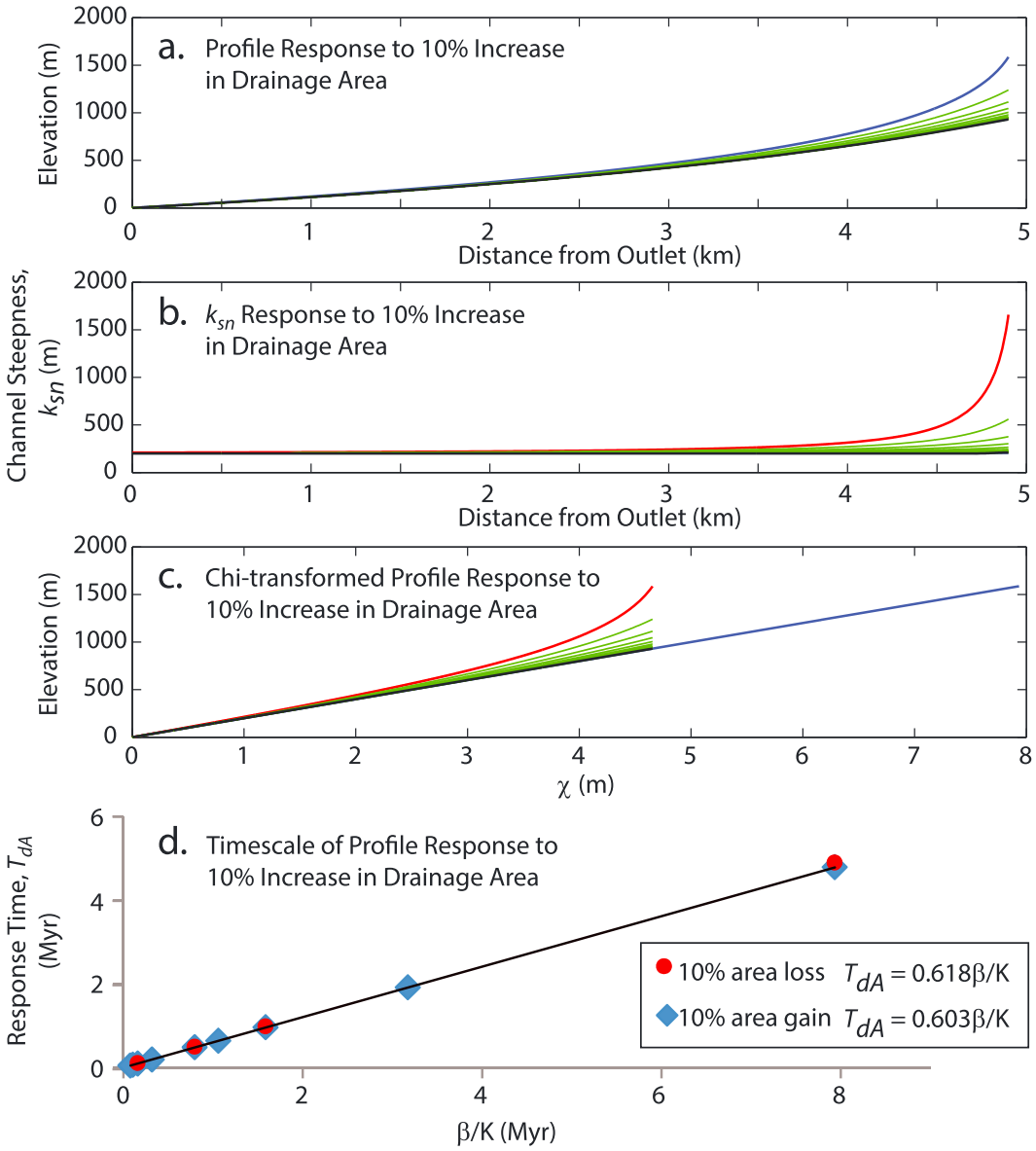

Figure 4. Channel response to an instantaneous area change: 1-D simulation. (a–c) Initial condition (blue lines) is a steady state channel with uniform $k_{sn} = 200$ ($K = 5 \times 10^{-6}$ yr^{-1}, $U = 0.001$ m yr^{-1}, $n = 1$, $m = ½$). The black lines are the final condition, and the green lines are intermediate states. In Figures 4b and 4c the red line represents the condition immediately following the area change; it is absent from Figure 4a because it takes time for the elevation to change and thus the red and blue lines are the same in this panel. In Figures 4b and 4c the blue and black lines (initial and final conditions) are collinear; equilibrium has been restored. Model output includes (a) river profiles, (b) along stream channel steepness (k_{sn}), and (c) χ-transformed river profiles. A 10% drainage area increase (added at the channel head) is imposed at the start of the model run and the χ-transformed profile and along stream pattern of k_{sn} change immediately, as expected (red lines). Only the channel downstream of the capture point is modeled. Green lines (nine time steps) show model output every 100 kyr after the change in drainage area, illustrating the return to the initial steady state form in just ~1 Myr (black line). The approach to steady state is asymptotic; after 500 kyr individual time steps cannot be visually discerned. (d) Response times for both a 10% area gain and a 10% area loss from 12 simulations are plotted against β/K. Results are described exactly ($R^2 = 1$) by equation (10), with a slight difference in $G(f_A)$ between the area gain and area loss scenarios.

Channel response to drainage area change and divide migration are not, however, independent in nature as they are in the simulations presented in Figures 5 and S2. A critical question is, what dictates the divide migration number, N_{Dm}, in natural systems? To evaluate the extent and pattern of river profile response in realistic scenarios, and quantify the controls on divide migration rate and thus the timescale over which divide

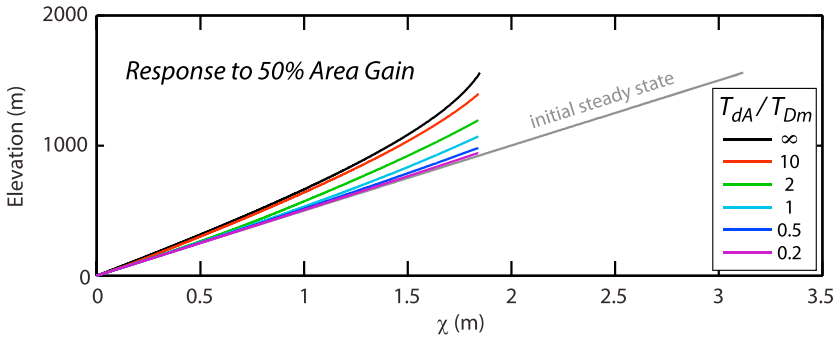

Figure 5. Channel response to a 50% drainage area gain as a function of the divide migration number, $N_{Dm} = T_{dA}/T_{Dm}$. One-dimensional river profile simulations for variable N_{Dm}, controlled by specifying T_{Dm}, the timescale over which divide migration (or drainage area change) is accomplished. Here drainage area is added at the channel head of an initially steady state river profile (grey line) at a constant rate during the simulation. In each case, χ-transformed channel profiles are shown for an area gain equal to 50% of the initial drainage area. The black line shows the case of instantaneous area gain ($T_{Dm} = 0$) such that there is no erosional response.

migration is active, we ran a large suite of 2-D landscape evolution simulations with FastScape [*Braun and Willett*, 2013] in which an initially steady state landscape with uniform rock uplift rate and erosional efficiency is subject to a perturbation to the pattern and magnitude of rock uplift orthogonal to the main drainage divide such that a period of divide migration is triggered. Although not presented here, it may be anticipated that qualitatively similar results would be obtained by varying the pattern of erosional efficiency [e.g., *Giachetta et al*., 2014]. We evaluated a subset of analogous models with CHILD [*Tucker et al*., 2001] (using our own simulations) and DAC [*Goren et al*., 2014] (viewing animations of simulations published in *Willett et al*. [2014]) to confirm that the rates and styles of landscape evolution are robust across model formulation and numerical integration schemes. All models behaved in an analogous manner, and we present here only FastScape models where the spatial pattern of rock uplift was perturbed, similar to the scenario modeled by *Willett et al*. [2014] using DAC.

Simulated landscapes presented here and in the supporting information all have open boundaries at model north and south, invariant erosional efficiency, *K*, and all were subjected to the following history of tectonic forcing: (1) a spatially uniform rock uplift rate for a sufficiently long time to establish a steady state where $E = U$ everywhere with stable divides, (2) a tectonic perturbation where the spatially uniform rock uplift pattern is replaced by a linear south-to-north gradient of increasing rock uplift rate for sufficiently long to reestablish steady state and restabilize the main divide (tilting phase), and (3) a return to the initial uniform rock uplift rate for sufficiently long for the main divide to return to its initial position and once again reestablish steady state with stable divides (return phase). Figure 6 illustrates typical model behavior using the case with $n = 1$ and $K = 10^{-5}\,\mathrm{yr}^{-1}$ (cases with $n = 2$ are visually indistinguishable; an example is shown in Figure S3 for completeness).

Simulations with both a tilting phase and a return phase in FastScape have one challenge: the channel network formed in the wake of migrating divides tends to be characterized by straight, parallel channels. The resulting change to Hack's law alters steady state profiles and impacts stable divide positions such that the main divide does not return to its original position at the end of the return phase. We found that including a realistic hillslope diffusivity coefficient, *D* ($0.0005 \le D \le 0.05\,\mathrm{m}^2\mathrm{yr}^{-1}$), and a fixed *K*/*D* ratio (0.002) eliminated this problem for simulations with $n = 1$. We could not, however, eliminate this problem for simulations with $n = 2$ and thus simulate only the tilting phase with $n = 2$. Fortunately, as shown below there was no detectable influence of diffusivity on drainage divide migration rate in our simulations. Simulations spanned a wide range of erosional efficiency, *K*, (Table 1) and thus steady state relief. We used this wide range of *K* to fully test the dependence of divide migration timescale on *K*, rather than to bracket a range of k_{sn} or steady state relief in our models, although this range of *K* does reflect the range determined in field calibration studies [e.g., *Stock and Montgomery*, 1999; *Kirby and Whipple*, 2012; *Lague*, 2014].

All models exhibited analogous behavior and the same dynamic range of main divide position, differing only in the timescale of divide migration. In all simulations there is a rapid initial landscape response during which

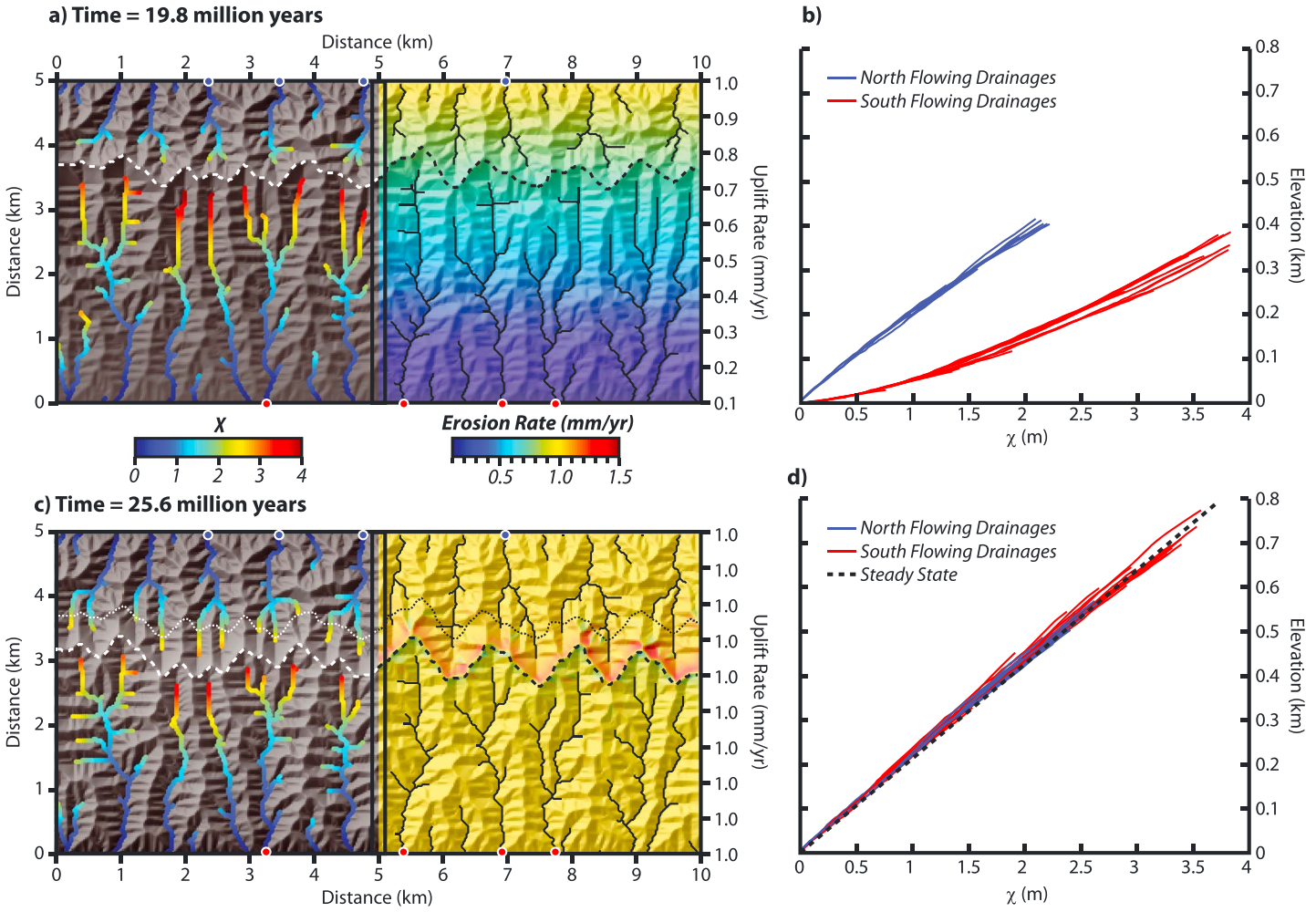

Figure 6. Data from two selected time steps from a FastScape simulation meant to largely mimic the model setup in *Willett et al.* [2014]. For each time step, (a, c) a hillshade map of the entire model domain, but split such that the left half of the domain shows streams colored by their χ value, while the right half of the domain is colored by erosion rate. (b, d) The χ-transformed profiles of the four largest rivers (outlets marked by dots) flowing to the top (blue) and the bottom (red) edges of the domain. River mouth locations are marked by colored circles on the map. (a, b) At steady state with a linear increase in rock uplift rate from bottom to top, reflected in the pattern of erosion rates (Figure 6a, right half). Thick dashed line marks divide location. Steady state χ-transformed profiles (Figure 6b) are curved in response to the spatial gradient in rock uplift rate and their spread reflects variations in channel orientation and catchment shape and thus in the relationship between χ and uplift rate. (c) Map for model time step halfway through migration of divide back toward the center of the model domain after rock uplift rate is changed to a uniform 1 mm/yr after reaching the steady state shown in Figures 6a and 6b. Thick dashed line marks current divide position, thin dashed line marks former stable divide position in (Figure 6a). (d) χ-transformed river profiles at same time step as in Figure 6c. See text for further discussion and Movie S1 in supporting information. Black rectangle at centerline of Figures 6a and 6c indicates location of swath profile in Figure 7 and Movie S2.

river profiles adjust to the tectonic perturbation, achieving approximately steady state forms largely before divide migration begins (Movie S1). This occurs on a timescale similar to the response time for a change in uplift rate—divide migration begins only once the change in tectonic boundary conditions manifests in a cross-divide difference in erosion rate (at time steps 0.8 Myr in the tilt phase and 20.8 Myr in the return phase; Figure 7 and Movie S2). Thus, divide mobilization is delayed until the response in channel profile form reaches at least one side of the divide. The timescale of this initial channel profile response to the change in tectonics is well described by T_{dU} (equation (8a)). As river profiles on one side or the other attain quasi steady forms, a contrast in erosion rate and channel elevation at a reference drainage area (and thus headwater slopes) develops, and divide migration is triggered in earnest. Thus, it is the contrast in river profile elevation across the divide that fundamentally drives divide migration. Divide migration rate rapidly increases to a peak at the end of initial channel profile response then gradually decreases as divide migration continues for more than an order of magnitude longer than the initial channel profile response (Figure 7 and Movie S2). As illustrated in Figure 7, the cross-divide erosion rate contrast is much higher than the cross-divide contrast in rock uplift

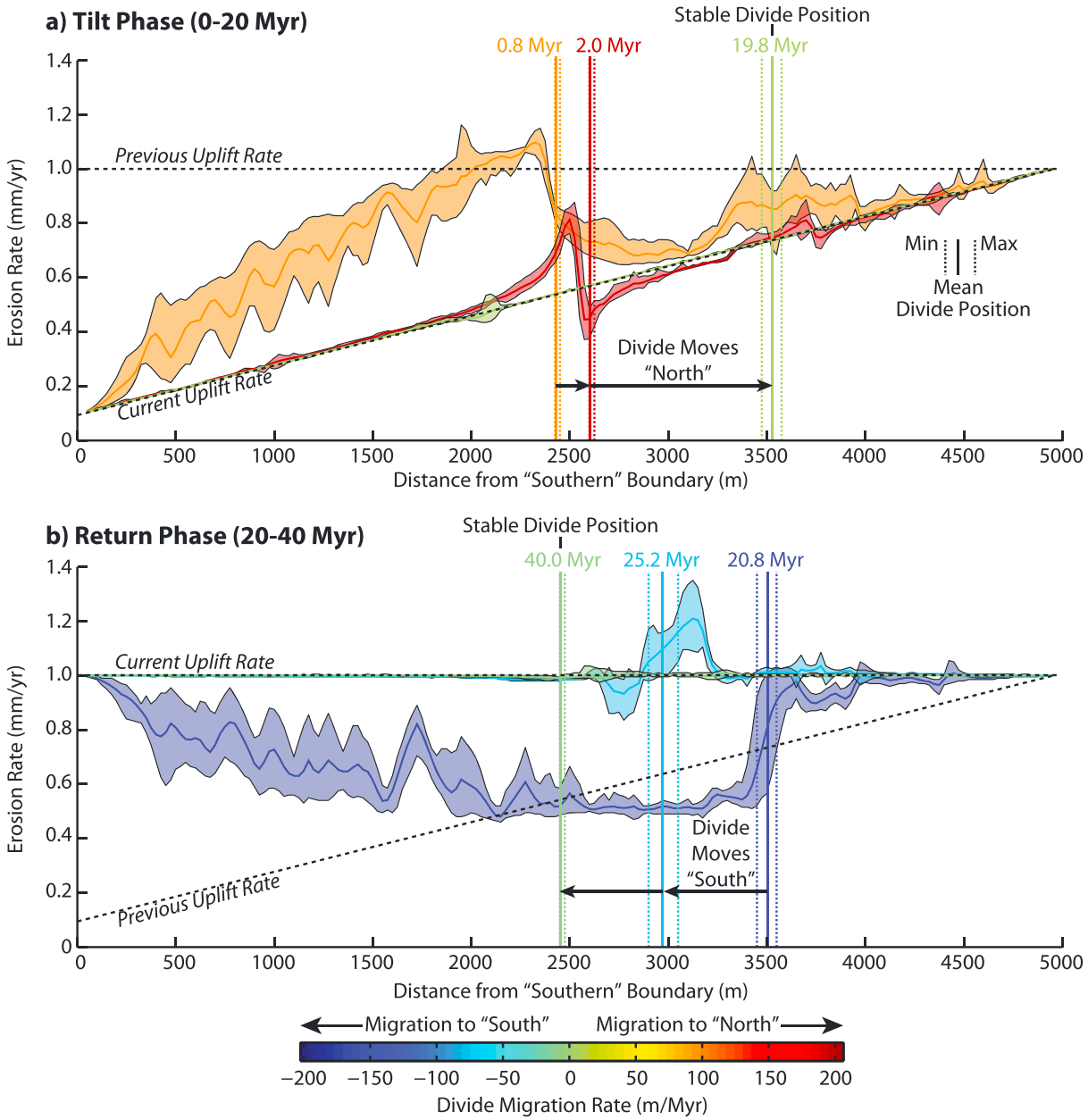

Figure 7. Swath profiles through FastScape results presented in Figure 6 at three time steps during the (a) tilt phase and the (b) return phase showing mean erosion rates (solid colored lines) and minimum and maximum rates (colored shaded areas). Swaths are 200 m wide and located at the center of the model domain (see Figures 6a and 6c). Solid vertical lines are mean positions of the drainage divide, and dotted vertical lines are minimum and maximum divide positions within swath. Black arrows highlight divide migration between time steps shown. Stable divide positions obtained at the end of the tilt (19.8 Myr) and return (40.0 Myr) phases are indicated. Coloring of divide positions and erosion swaths are keyed to the divide migration rate at that time step (scale at bottom of figure) with positive migration rates indicating motion "northward" and negative migration rates indicating motion "southward." Black dashed lines indicate current and former spatial patterns in uplift rate during the respective phases. The time of each displayed time step is shown above the divide position. (a) Tilting phase: initial condition is uniform uplift (previous uplift rate) and erosion. Time steps shown are (1) the moment the initial channel profile response to the tectonic perturbation has reached the divide (0.8 Myr), (2) during rapid divide migration (2.0 Myr), and (3) at quasi steady state (19.8 Myr) where erosion rates closely match uplift rates everywhere (the initial condition for the return phase). (b) Return phase: as per Figure 7a with time steps shown (1) the moment the initial channel profile response to the tectonic perturbation has reached the divide (20.8 Myr), (2) during rapid divide migration (25.2 Myr), and (3) at quasi steady state (40.0 Myr) where erosion rates closely match uplift rates everywhere (equivalent to the initial condition for the tilt phase). Note the strong cross-divide contrast in both erosion and thus net surface uplift (uplift – erosion) that develops after the initial channel response to tectonic perturbation (0.8 and 20.8 Myr). These contrasts drive divide migration (see also Movie S2).

rate during landscape response and active divide migration. Conversely, divides can stabilize despite a spatial gradient in rock uplift rate once rivers in the landscape equilibrate to steady state forms.

Consistent with the observation that channel profiles adjust much faster than the main divide moves, χ-transformed river profiles throughout the simulations exhibit only very slight "area gain" and "area loss" perturbations, flickering slightly and rapidly about the expected steady state condition (Figure 6d and Movie S1). Despite these quasi steady river profile forms, there is a persistent increase in erosion rate at the tips of aggressor streams and commensurate decrease in erosion rate at the tips of victim streams that results in divide migration (Figures 6c and 7 and Movie S2). Because of the much faster adjustment of channel profiles back to quasi steady forms, perturbations associated with drainage area change (Figure 2a) never grow, however, and the positive feedback mechanism described by *Willett et al*. [2014] is not manifest in evolving channel profiles. Instead, the negative feedback of channel profile form response to differential erosion rates (black and grey arrows, Figures 2b and 2c) dominates system behavior, implying that the divide migration number, N_{Dm} (equation (6)), is much less than unity in all our simulations (Figure 5).

To quantify the divide migration timescale and determine the controls on N_{Dm}, we ran simulations of landscapes with both $n=1$ and $n=2$ and with a wide range in erosional efficiency ($10^{-4} \le K \le 10^{-6}\,\mathrm{yr}^{-1}$ for $n=1$ and $10^{-5} \le K \le 10^{-8}\,\mathrm{m}^{-1}\mathrm{yr}^{-1}$ for $n=2$) and maximum rock uplift rate ($5\times10^{-4} \le U_{\mathrm{max}} \le 5\times10^{-2}\,\mathrm{m\,yr}^{-1}$ for $n=1$ and $5\times10^{-4} \le U_{\mathrm{max}} \le 10^{-2}\,\mathrm{m\,yr}^{-1}$ for $n=2$) (Table 1). All simulated landscapes were subjected to the same history of changing rock uplift rate patterns relative to U_{max}. These simulations and plots of the time history of divide migration rate during both "tilt" and "return" phases (Figure S4) reveal that divide migration rate declines exponentially with time after it peaks at the end of the initial channel profile response to the tectonic perturbation discussed above (as noted above only the tilt phase is considered for cases with $n=2$). Divide migration rate asymptotically approaches zero as the main divide reaches its equilibrium position (Figure S4). Exploiting intuition developed in prior analyses of river profile response time dependencies on variables β, K, U, m, and n (equations (8)–(10)), we used regression analysis of the time history of divide migration rate to discover the form of the divide migration timescale equation. We find that divide migration rate, D_{mr}, decays exponentially from its peak, $D_{\mathrm{mr\_max}}$, according to

$$D_{\mathrm{mr}} = D_{\mathrm{mr\_max}} e^{-b\beta^{-1}K^{1/n}U^{[1-(1/n)]}t} \tag{12}$$

where b is a constant. The peak migration rate scales with $K^{1/n}U^{[1-(1/n)]}$ (Figure S5) but does not influence how long it takes the divide to reach a new equilibrium position. For the range of hillslope diffusivity coefficients and the model grid size (25 m) used in our simulations, we find almost no difference in T_{Dm} between models with and without hillslope diffusion for both $n=1$ and $n=2$ (Figure S6). As with all problems of exponential decay, the timescale of divide migration, T_{Dm}, scales with the e-folding time of the decay of D_{mr}. As divide migration rate is near 0 after three e-folding times, we define the divide migration timescale as three times the e-folding time (a conservative minimum estimate of T_{Dm}):

$$T_{\mathrm{Dm}} = 50.2\beta K^{-1/n}U^{[(1/n)-1]}; n=1 \tag{13a}$$

and

$$T_{\mathrm{Dm}} = 25.6\beta K^{-1/n}U^{[(1/n)-1]}; n=2, \tag{13b}$$

where 50.2 and 25.6 (equal to $3/b$) are empirical constants found by regression of model results. Note that the form of equations (13a) and (13b) is general (applies for all n); only the prefactor is specific to the value of n (evaluated here for $n=1$ and $n=2$ only). Importantly, comparing equations (10), (13a), and (13b) reveals that T_{Dm} and $T_{\mathrm{d}A}$ scale in precisely the same way with β (set by m/n, initial basin length, shape, and drainage density, equation (9)), K, and U for all n (and thus m for a given m/n ratio). Both T_{Dm} and $T_{\mathrm{d}A}$ are about twice as long for $n=1$ than for $n=2$, but the divide migration number, N_{Dm}, given by the ratio of timescales, $T_{\mathrm{d}A}/T_{\mathrm{Dm}}$ is a constant much less than unity:

$$N_{\mathrm{Dm}} = 0.017, \tag{14}$$

for both $n=1$ and for $n=2$ (see Figure 8). The finding that the timescale of divide migration is much longer than profile equilibration time was also reported by *Willett et al*. [2014] on the basis of simulations with DAC. In our simulations, the timescale of channel profile response to changes in drainage area is always much less than the timescale of divide migration (Figures 8 and S7). Thus, for the parameter space evaluated, landscapes exist in a state where perturbation of channel profiles away from equilibrium in response to drainage

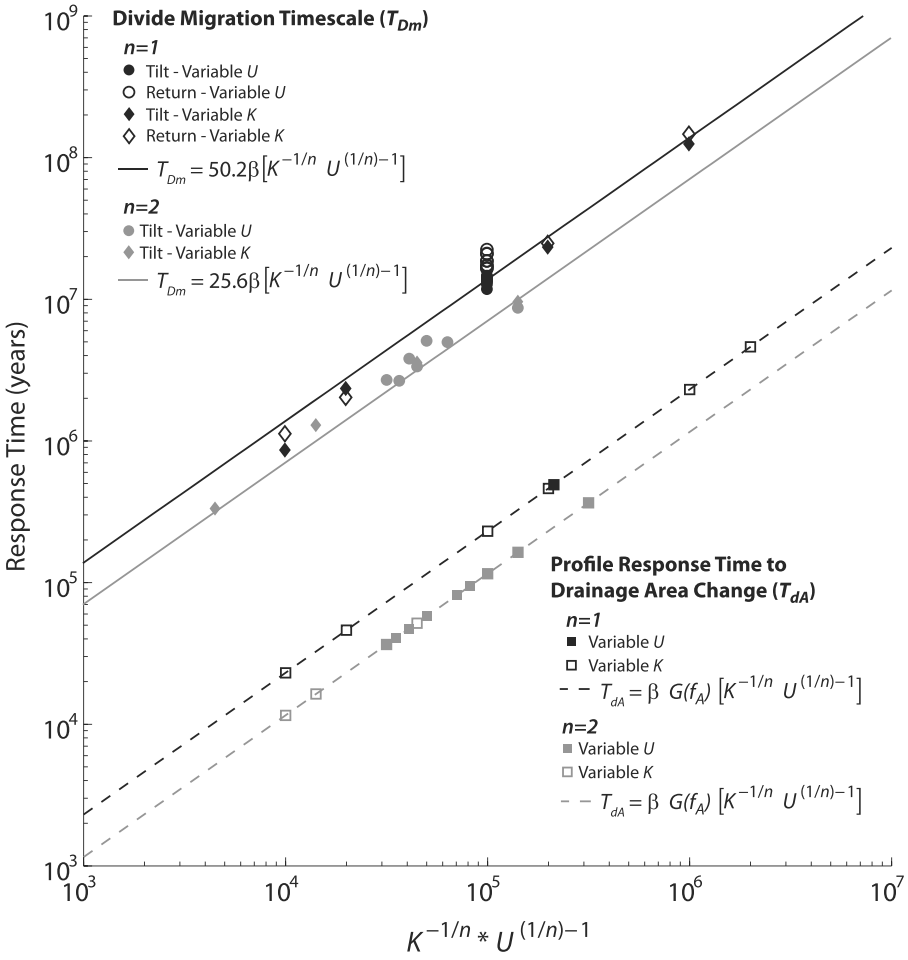

Figure 8. Timescales of divide migration (T_{Dm}) and channel profile response to drainage area change (T_{dA}) as a function of model parameters (β, K, U, m, and n; m/n held fixed). Different symbols mark T_{Dm} and T_{dA} in simulations with either $n = 1$ or $n = 2$ and for experiments in which either K or U was varied (see Figures 4, 6, and S3 for examples). Note that in both cases for $n = 1$, there is no dependence on U (points plot on top of each other, within scatter for T_{Dm}). There is a slight difference in T_{Dm} in the tilt and return phases, owing to changes in channel network structure (and thus β). We show T_{dA} for a 10% change in total drainage area. Because T_{dA} decreases with increasing fractional area change (equation (11)), this is a conservative measure of channel profile response time for significant area change. Note the divide migration number, N_{Dm}, defined by the ratio of T_{dA} to T_{Dm} (equation (6)) is always much smaller than 1. Figure S7 replots these data into two figures to illustrate in isolation the dependence of T_{Dm} and T_{dA} on K and U.

area gain or loss (as illustrated in Figure 2a) via progressive divide migration will be negligible, below the level of detection, as illustrated by the evolution of χ-transformed river profiles in our simulations (Figures 6 and S3 and Movie S1).

4.3. Timescales and Patterns of Landscape Response to Discrete Capture Events

Large discrete drainage capture events are most likely to significantly perturb channel profile forms and produce readily interpretable signatures of area gain and area loss (Figure 2), as illustrated, for example, by *Willett et al.* [2014] for the capture of the Apalachicola headwaters by the Savannah river. Large capture events like these are not favored in scenarios like that considered in section 4.2 where gradients of rock uplift rate or erosional efficiency drive progressive divide migration essentially parallel to the orientation of major drainage lines on either side of the range crest divide. In contrast, headward erosion of short, steep catchments oriented orthogonal to preexisting long, narrow catchments is likely to trigger a sequence of large drainage capture events. Here, we explore the degree to which signatures of drainage area change from discrete capture are expressed in settings characterized by headward advance of small streams oriented orthogonal to the grain of the major drainage lines.

To create such a scenario in FastScape, we first built a steady state landscape with uniform uplift draining only to the south then later opened the east and west boundaries to outflow. A narrow nonuplifting strip along east and west boundaries was maintained prior to opening of those boundaries to prevent abrupt formation of waterfalls along model edges at the moment the boundaries were opened to flow. An initially south-tilting plain ensured the development of long, narrow, parallel drainages over most of the model domain. After opening of the east and west boundaries, a systematic lateral narrowing of central catchments by progressive east-west divide migration ensued. The process of divide migration included a sequence of abrupt divide shifts associated with significant drainage capture events (Figure 9 and Movie S3). As expected [*Willett et al*., 2014], large drainage capture events are marked by dramatic warping of χ-transformed river profiles reflecting both area loss and, especially, area gain (Figures 2 and 9b). In our models, even these large perturbations to river profile form were rapidly erased (Figure 9d and Movie S3). The timescale of river profile response to abrupt changes in drainage area is well described by equations (10) and (11), as demonstrated above. Thus, our analysis implies that landscapes characterized by large capture events during major reorganization of the drainage network will indeed occasionally express clear area gain and area loss signatures, but these landforms will be short-lived and thus fairly rare. The likelihood of preservation of such signatures in the modern topography is described by the drainage capture number, N_c (equation (7)), defined above as the ratio of the timescale of channel profile response, T_{dA}, and the characteristic recurrence interval between large capture events, T_c. T_c will likely depend on the particulars of the geologic, climatic, and tectonic conditions that have conspired to induce a major drainage reorganization capable of inducing a period of recurrent large drainage capture events [e.g., *Prince et al*., 2010, 2011], but otherwise will be dictated by the rate of advance of the aggressor network, similar to the controls on T_{dU}, T_{dA}, and T_{Dm}. Systematic exploration of the controls on T_c and the various scenarios of geologic contingency (such as those illustrated in Figure 9 and in *Yang et al*. [2015]) that set up the potential for repeated large drainage captures is beyond the scope of this paper but is a potentially fruitful area of future research.

Importantly, the stream captures highlighted above usually involve a headwater reach made susceptible to capture through the area loss feedback. During vigorous divide migration perpendicular to the main topographic grain, isolated catchments encroached from all sides can develop, allowing the positive area loss feedback to locally keep pace with the negative channel-response feedback (see Figures 1 and 2). This is best seen in Movie S3 in later stages of the simulation (>8 Myr) but is also expressed in several catchments in which headwater erosion rates are suppressed below the uplift rate in Figure 9. Movie S3 shows that these catchments maintain a clear area loss signature on χ-transformed profiles as they are rapidly encroached from all sides, as has been described by *Goren et al*. [2014], *Willett et al*. [2014], and *Yang et al*. [2015]. Between 10 and 15 Myr in the simulation, the center catchment loses 10% of its area every 0.5 Myr, defining T_{Dm} for a 10% area change. Using our 1-D profile model and the size and shape of this catchment during this time interval, we find an average T_{dA} for a 10% area change of 0.42 Myr. This implies $N_{Dm} \sim 0.84$, consistent with the analysis in Figure 5. The difference between the simulations in Figures 9 and 6 shed some light on the circumstances under which the positive area loss signature is likely to be preserved in river profiles and those under which it is not. The frequency of occurrence and longevity of such catchments will likely depend, as noted above, on erosional efficiency and conditions of geologic contingency that can trigger network instability.

5. Topographic Metrics for Recognizing Mobile Divides

Willett et al. [2014] proposed that χ anomalies (contrasting χ values across divides) provide a simple metric of divide instability. This method is elegant in its simplicity and has several highly appealing characteristics: (1) maps of χ are easily computed, even for very large areas, (2) maps of χ are not sensitive to DEM resolution and noise (barring occasional errors in routing of large drainages), (3) χ anomalies are readily identified at a glance at even large regional scale, and (4) it has been used successfully to identify capture locations and mobile divides in both the Appalachian Mountains and the Central Range of Taiwan [*Willett et al*., 2014]. The principle behind interpretation of cross-divide χ anomalies as a metric of divide instability, however, reveals the restrictive assumptions upon which the method rests. A unique relationship between χ at the channel head and actual channel head elevations throughout the study area exists if and only if (1) rock strength and the history of erosivity, K, and rock uplift rate, U, are spatially uniform, (2) transient response to any changes in K or U is well described by the detachment-limited stream power model [e.g., *Kirby and Whipple*, 2012], and (3) all catchments analyzed have the same outlet elevation (Figure 3). Although in principle such effects could be

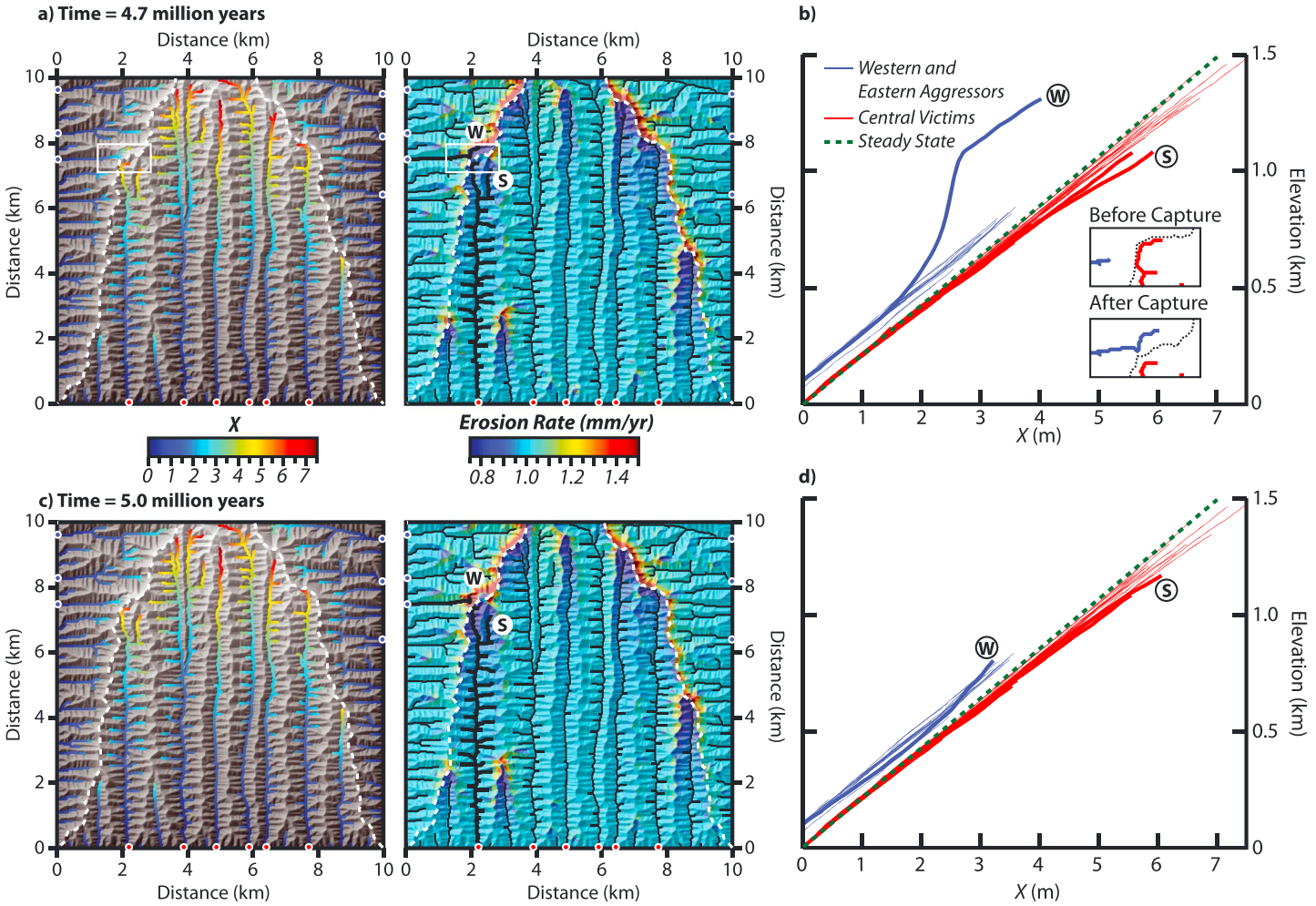

Figure 9. Two selected time steps of a FastScape simulation of lateral divide migration illustrating the effects of a sudden large stream capture event. The (a, b) first time step is immediately after the capture event, and the (c, d) second time step is just 0.3 million years later. In Figures 9a and 9c the left column is a hillshade of the model topography colored by elevation with streams colored by their χ value, and the right column is a hillshade of model topography colored by erosion rate. Dashed white lines show divide positions. Two streams in the right (erosion rate) panels of Figures 9a and 9c are highlighted with thick black lines, a "western" aggressor (W) and a "central," south-draining victim (S). (b) The χ-transformed profiles for selected streams; stream mouths are marked in the map, with the western and eastern aggressors in blue and central victims in red. Expected steady state profile shown as dashed green line. The two streams highlighted on the erosion rate maps are in bold and marked with (W) and (S). Inset in the bottom right shows a map view of the stream network in the preceding time step (before capture) and in the displayed time step (after capture). Dashed line is divide position; location of small map is indicated with a white box on the map (Figure 9a). (d) The χ-transformed profiles for time step shown in Figure 9c, setup is identical to Figure 9b. See text for further discussion and Movie S3 in the supporting information.

accounted for [*Willett et al.*, 2014], in practice, this is rarely possible both because the many controls on K remain poorly quantified and because the stream power model does not capture the full richness of river profile evolution. Thus, only if these assumptions hold is an across-divide χ anomaly an effective proxy for a contrast in channel head elevations and an associated difference in mean headwater slope or relief that will establish differential erosion rates and drive the divide form low channel-head χ toward high channel-head χ.

Interpreting χ anomalies as a metric of divide mobility, however, can be misleading in any circumstance where the assumptions of spatially invariant histories of U and K and a common outlet elevation of all catchments under consideration are violated. Unfortunately landscapes that satisfy these restrictive assumptions are rare. Spatial variability in one or more of outlet elevation, rock strength, climatic history, or rock uplift rate history is important in most landscapes. The strong χ anomalies across the main divide under steady state and stable divide conditions in our models with a south-north rock uplift rate gradient is a simple example (Figure 6). Similar conditions will result from gradients in climate or rock strength [*Giachetta et al.*, 2014]. These potentially confounding, but common, complications lead us to evaluate other potential metrics of divide instability.

We consider alternative metrics that are (1) not contingent on restrictive assumptions about downstream conditions and (2) directly related to the immediate driver of divide migration: different erosion rates on either side of a drainage divide [*Gilbert's* [1877] law of unequal slopes]. We use our 2-D landscape evolution simulations from section 4.2 (Figure 6 and Movie S1) to evaluate the potential utility of cross-divide contrasts in (1) mean headwater erosion rate, which is proportional to channel steepness, mean hillslope gradient (if below-threshold values), and mean local relief assuming no difference in the erosion rate constant, K, across divides; (2) headwater mean slope; (3) headwater mean local relief; (4) channel elevation at a reference drainage area (e.g., 0.1–1 km^2); and (5) χ at the same reference drainage area (Figure 10). Actual channel head locations are difficult to determine from topography alone [*Montgomery and Foufoula-Georgiou*, 1993; *Passalacqua et al*., 2010; *DiBiase et al*., 2012; *Clubb et al*., 2014], but for our purposes this is unnecessary. To characterize cross-divide contrasts in channel head elevation and χ, we need only measure both metrics at a consistent reference drainage area. We use a reference area of 0.1 km^2 in all analyses of our simulated landscapes. This reference drainage area is embedded within all the metrics, as all metrics are either calculated at the reference drainage area or in the contributing area above the reference drainage area (e.g., mean erosion rate, mean slope, and mean local relief). Additionally, the calculation of headwater mean local relief includes only elevations within the catchment of interest.

All metrics except the χ anomaly show consistent, quasi-linear relationships with the mean rate of main-divide migration throughout model runs, with cross-divide contrasts reducing to near zero as the main divide reaches a stable position (Figure 10). Steady divide positions (zero migration rate) in the return phase with uniform rock uplift rate are associated with negligible cross-divide contrasts in all metrics except channel elevation at the reference drainage area (the result of cross-divide differences in headwater basin shape created in the prior divide migration phase). During the initial channel profile response to tectonic perturbation at the start of either the tilting or the return phase, cross-divide contrasts in all metrics (except channel head χ) and thus divide migration rate rapidly increase to maxima (first six time steps shown, Figure 10). Once the initial channel profile adjustment to tectonic perturbation is complete, divide migration rate (and direction) is linearly related to the magnitude of cross-divide differences in all metrics and, except for cross-divide contrasts in χ, these differences are steadily reduced by divide migration, which occurs at an ever decreasing pace. Small cross-divide contrasts in all metrics (channel elevation at the reference drainage area, mean headwater erosion rate, hillslope angle, and local relief) at the end of the tilting phase are sustained by the cross-divide difference in rock uplift rate. The evolution of the χ anomaly is similar except that in the tilting phase when divide migration is driven by the imposed gradient in rock uplift rate, the χ anomaly steadily increases during divide migration after the initial channel profile response to the tectonic perturbation. Additionally, the steady state cross-divide χ anomaly supported by the imposed rock uplift rate gradient is the largest magnitude χ anomaly obtained.

Given the equivalent behavior of all metrics tested above besides the χ anomaly, it is worth considering which metric is likely the most useful for application in nature. A direct measure of cross-divide differences in mean headwater erosion rates will always be best, but is expensive and time-consuming to determine. Our preferred topographic metric is mean headwater local relief because it is easily determined, well correlated with mean hillslope angle and channel steepness, but typically less locally variable than either because relief is insensitive to noisy elevation data. Moreover, mean hillslope angle attains threshold values at high erosion rates and therefore becomes an ineffective metric of erosion rates in many tectonically active settings [e.g., *Ouimet et al*., 2009; *DiBiase et al*., 2010].

6. Application to a Natural Landscape

One way to test the implications of our model simulations and quantification of relative timescales of divide migration and channel response is to evaluate the degree to which independently identified aggressor and victim streams on either side of a divide express area gain and area loss signatures, respectively (Figure 2). A striking example of a catchment that appears to be gaining area by encroachment into flanking catchments on either side has been identified by *Willett et al*. [2014] near the crest of the Taiwan Central Range (Figure 11). The interpretation that this catchment is gaining area at the expense of its neighbors is supported by the unusually narrow shape of flanking catchments, the higher elevation of river beds in both flanking catchments, the presence of numerous wind gaps indicating the greater former extent of the flanking catchments

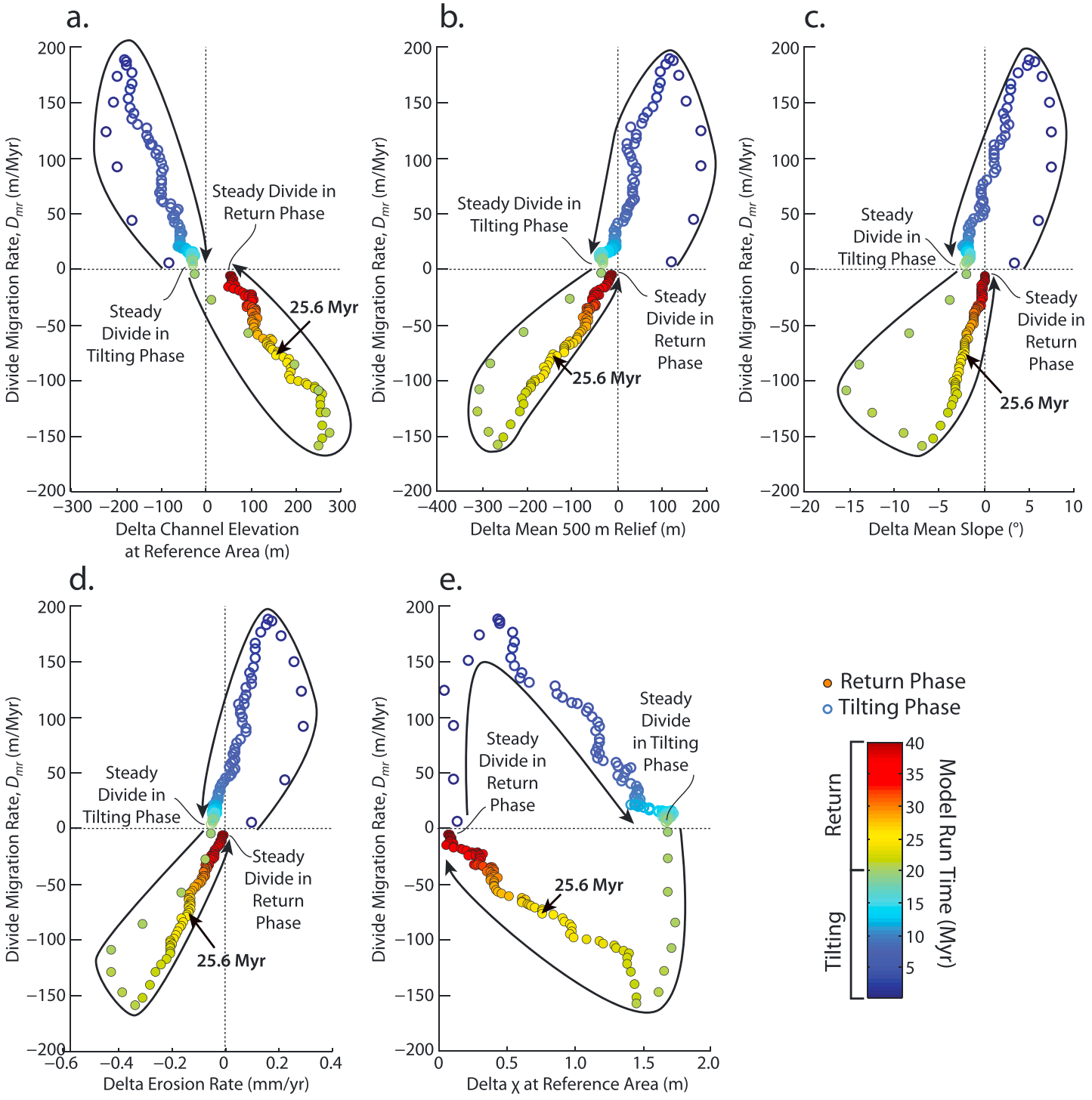

Figure 10. Comparison of divide instability metrics during the FastScape simulation shown in Figure 6. Location of time step 25.6 Myr corresponding to Figures 6c and 6d is indicated. For each plot, individual time steps are colored by the model run time, and hollow circles are time steps during the tilting phase (0–20 Myr) where the model is driven by a spatially variable uplift rate to force divide migration, and solid circles during the return phase (20–40 Myr) when this spatially variable uplift rate is replaced by a constant uplift rate. Temporal progression is also highlighted schematically by long curving black arrows. *Y* axis in all plots is divide migration rate, D_{mr}, in m/Myr, with positive movement in the model Y-direction (north) defined as a positive divide migration rate. Values on *X* axes are the difference across the divide in (a) channel elevation, (b) mean 500 m local headwater relief, (c) mean headwater hillslope angle, (d) mean headwater erosion rate, and (e) χ value, all measured at, or averaged upstream from, a reference drainage area of 0.1 km^2. Note that models were run until divides were essentially stable with migration rates near 0, but slight cross-divide contrasts in all metrics persist suggesting runs did not reach an ultimate steady state with perfectly stable divides.

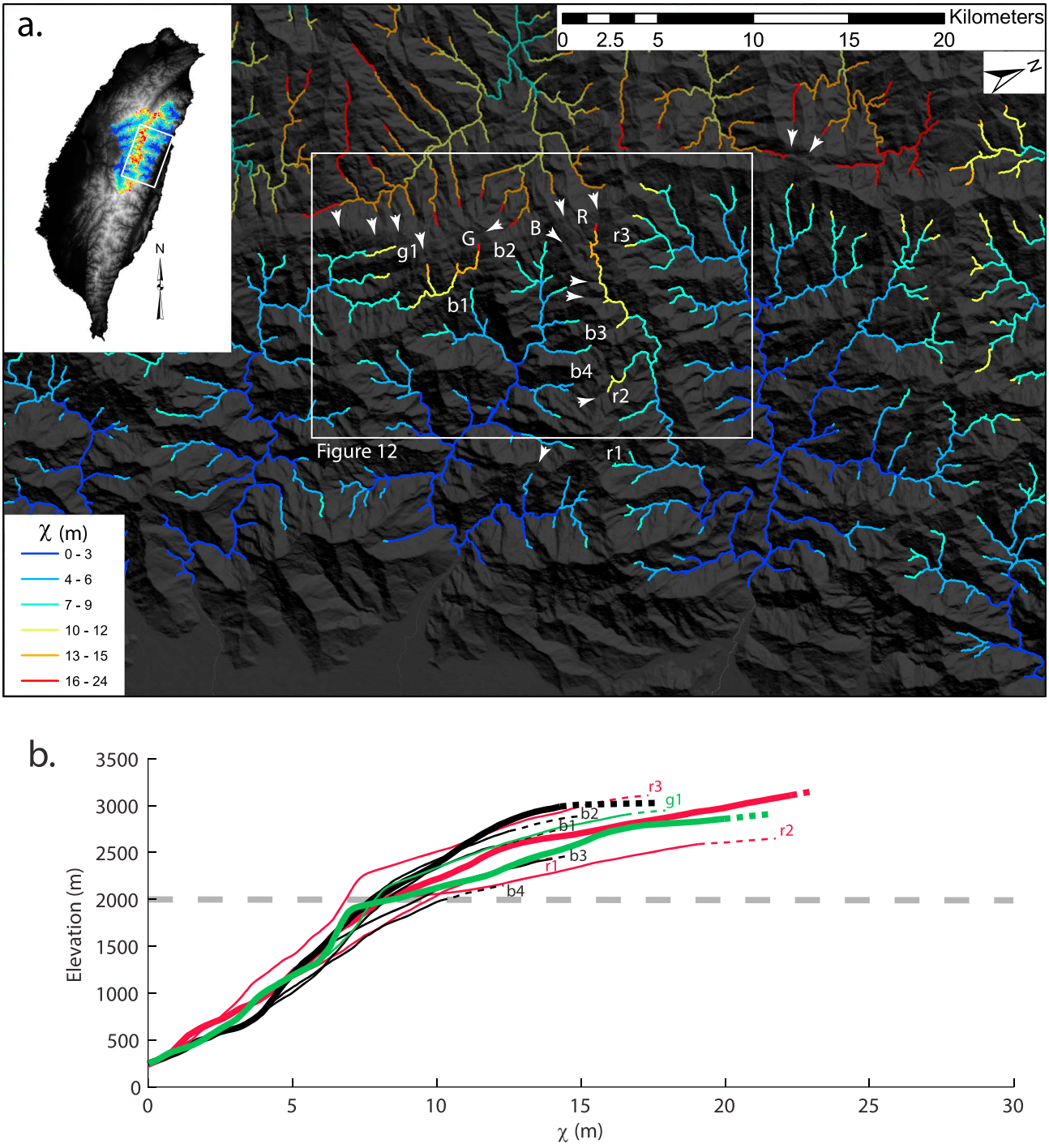

Figure 11. Natural example of catchments with unstable, evolving drainage divides in Taiwan identified by *Willett et al.* [2014]; inset shows location. (a) Hillshade map (dark) with streams colored by χ ($\theta_{ref} = 0.45$) and divide migration directions (white arrows) inferred from wind gaps identified visually with Google Earth. The χ values of west-flowing catchments are shown in faded colors because differences in rock type, mountain front elevation, and likely rock uplift rate on either side of the range crest are expected to invalidate interpretation of χ anomalies along the range crest which otherwise might be taken to suggest the wrong direction of divide migration. The central east-flowing catchment (mainstem B, tributaries b1–b4) is gaining area at the expense of adjacent catchments as suggested by χ anomalies between east-side catchments and documented in wind gaps. Location of Figure 12 indicated by box. (b) The χ-transformed river profiles from the central gaining catchment (black: mainstem (bold) and four tributaries; B, b1–b4 in Figure 11a) and adjacent losing catchments to the north (red: mainstem (bold) and three tributaries; R, r1–r3 in Figure 11a) and to the south (green: mainstem (bold) and one tributary; G, g1 in Figure 11a). Colluvial channel tips [*Montgomery and Foufoula-Georgiou*, 1993] are dashed. The χ-transformed river profiles are remarkably uniform, exhibiting a consistent decrease in k_{sn} above ~2000 m (dashed grey line). The mainstem of the aggressor catchment (bold black line) shows a slight warping over $10 < \chi < 13$ consistent with, but not necessarily diagnostic of, recent area gain, but no other profiles show any hint of an area gain or loss signature, consistent with expectation from our analysis of relative response timescales.

readily identified in Google Earth, and indications that erosion rates are lower across divides surrounding the catchment, as evidenced by higher channel bed elevations at comparable drainage area and lower hillslope angles, local relief, and channel steepness index (Figures 11 and 12). Figure 12 confirms expectations from our simulations about the utility of various metrics of divide migration direction. In every case the direction of divide migration is from low channel bed elevation to high, and from high local relief to low, as expected. Also, divide migration is consistently from low to high channel head χ only in catchments east of the range crest, as expected [*Willett et al*., 2014]. Local relief appears to be the most reliable metric for assessing the direction of divide migration (absent direct evidence from wind gaps). Estimating divide migration velocity, however, would require data on the spatial pattern of erosion rates or at least well-calibrated local correlations between topographic metrics and erosion rate.

Despite clear evidence for active divide mobility, a comparison of streams draining to either side of the divides reveals no indication of the expected systematic cross-divide differences in χ-transformed river profiles associated with aggressor versus victim catchments (Figure 2a). Indeed, all χ-transformed profiles examined exhibit very similar forms, with piecewise linear profiles characterized by steeper slopes (higher k_{sn}) below well-defined slope-break knickpoints near 2000 m elevation, regardless of position relative to the clearly mobile divides (Figure 11b). These river profiles appear to record an ongoing response to a temporal change in either rock uplift rate or erosional efficiency [e.g., *Wobus et al*., 2006; *Kirby and Whipple*, 2012; *Whittaker*, 2012] that is likely the ultimate cause of the observed drainage network rearrangement. This example supports our finding that because of the short timescale of channel adjustment to drainage area change, under most circumstances gradually migrating divides will not induce more than subtle curvature in χ-transformed river profiles in response to the gain or loss of drainage area.

Rather, drainage network dynamics are most likely to leave a clear and lasting imprint on χ-transformed river profiles (and thus equivalently slope-area relations and patterns of channel steepness, k_{sn}) wherever disequilibrium conditions favor major drainage capture events and especially so in such landscapes with low erosional efficiency (K). Moreover, the χ-transformed river profiles in Figure 11b confirm that the negative feedback wherein nonuniform erosion rate patterns tend to maintain quasi-equilibrium river profiles during active divide migration overwhelms the potential for area gain and loss effects to amplify cross-divide erosion rate contrasts and thus the rate of divide migration. Figure 12 highlights how divide migration direction is systematically correlated with cross-divide differences in local relief, channel head elevation, mean slope, and mean channel steepness, despite the absence of area gain/loss signatures in χ-transformed channel profiles. Consequently, the low relief (and thus erosion rate) character of the victim catchments is a driver and not a consequence of divide migration. This suggests that the interpretation of high-elevation low-relief surfaces experiencing progressive area loss to the surrounding deeply entrenched, rugged landscape presented by *Yang et al*. [2015] may have cause and effect reversed [*Whipple et al*., 2017].

7. Implications for Landscape Evolution

7.1. Potential for Mobile Divides to Influence Channel Long Profiles

Our analysis of river profile response time and 1-D river profile evolution models (both using the detachment-limited stream power model and restricted to active tectonic settings) predicts that the timescale of river profile response to drainage area change is far shorter than the timescale of gradual headward divide migration as might be driven by perturbations of the spatial pattern of rock uplift, rock erodibility, erosivity of the climate, or baselevel (Figures 4 and 8), suggesting that the imprint of divide mobility on topography will be subtle under these circumstances. Simulations with 2-D landscape evolution models confirm this expectation, showing that timescales of headward divide migration have the same sensitivity to model parameters K, U, m, n, and stream length L (encapsulated in β) but are more than an order of magnitude longer. Thus, gradual divide migration in response to sustained differences in erosion rate across divides triggered by tectonic, lithologic, baselevel, or climate perturbation does not appear likely to leave an interpretable signature in river profile forms (e.g., Figure 6 and Movie S1). Consequently, interpreting landscape history primarily through the lens of perturbations of χ-transformed river profiles expected to result from sudden drainage area gain or loss can lead to misunderstanding. Perturbations of χ-transformed river profiles (or equivalently slope-area diagrams or plots of k_{sn} versus streamwise distance) are more likely in the scenarios considered to result from spatial and temporal variability of rock strength, climate, and rock uplift rate. Our analysis applies

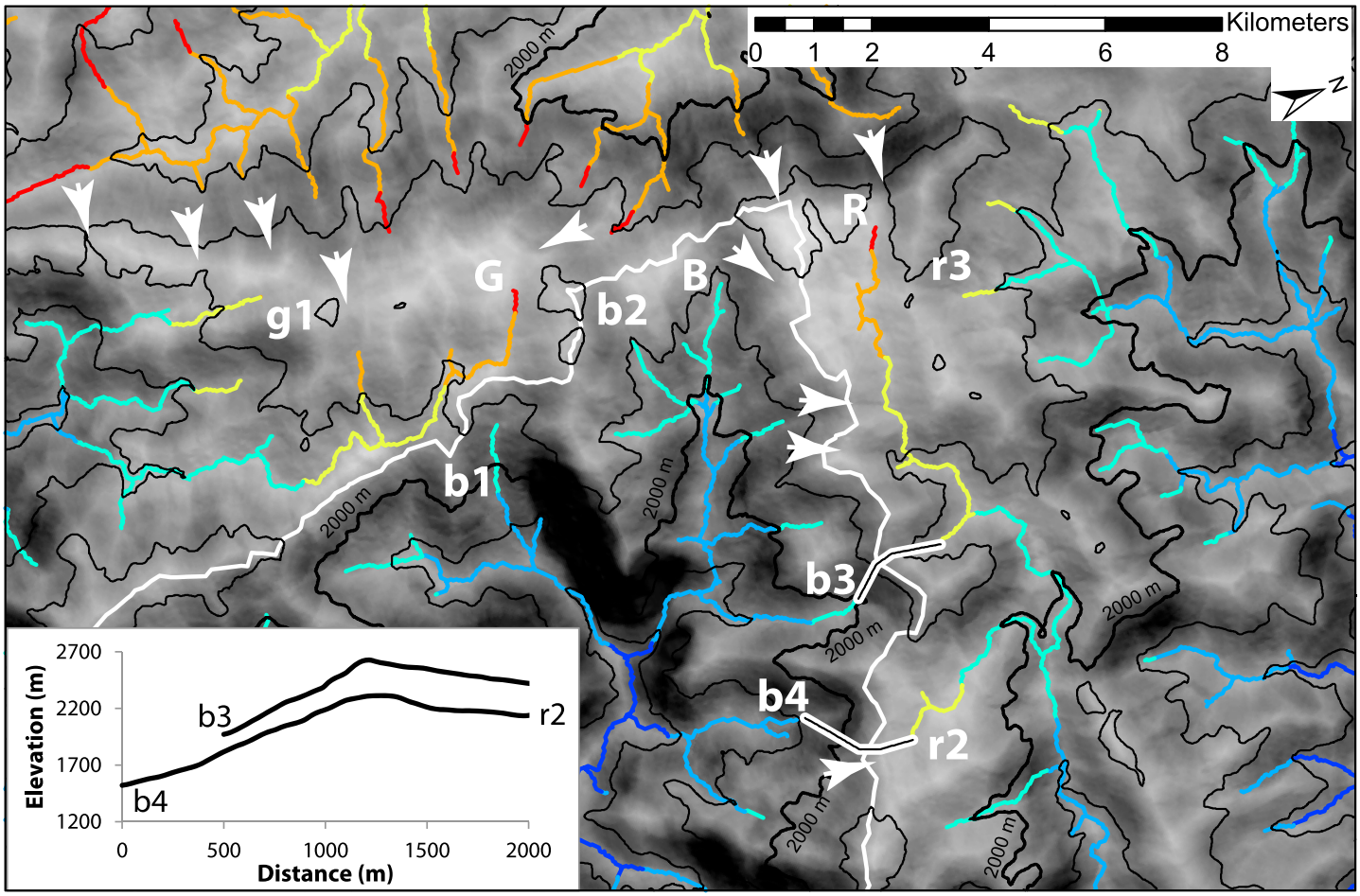

Figure 12. Illustration of alternative metrics for divide mobility. Zoom of Figure 11 with channels colored by χ (as in Figure 11), hillshade topography shaded by local relief (500 m radius, low values in lighter tones), 500 m contours in black (2000 m contour bold), expanding central catchment ("B") divide in white, and white arrows indicating divide migration direction from wind gaps, see Figure 11. Inset shows topographic profiles across the divide from 1 km^2 drainage area on tributaries b3 and b4 (profile locations in black with white halo). In every case direction of divide migration is from low channel head elevation to high and from high local relief to low, as expected. Also as expected only in catchments east of the range crest is divide migration consistently from low channel head χ to high.

to all rates of rock uplift (U) but does presume active uplift and that quasi-equilibrium is a natural attractor state. In slowly eroding postorogenic landscapes, this condition may be approached via isostatic rebound in response to erosional unloading, but complex patterns of rock erodibility have the potential to trigger drainage reorganization [e.g., *Prince et al*., 2010, 2011].

Circumstances most likely to preserve a clear signature of divide mobility or drainage area change through river capture are landscapes with low erosional efficiency (strong rocks, coarse bed material, and nonerosive climate conditions) subject to nonuniform tectonics and baselevel fall or characterized by spatially variable rock erodibility with the potential to trigger large drainage capture events. As nicely described by *Davis* [1903] and documented by *Prince et al*. [2010, 2011] and *Willett et al*. [2014] in the Appalachian Mountains, large, recent (relative to T_{dA}, the river profile response timescale) drainage capture events can and do occasionally leave a clear, diagnostic signature in river profiles and in the record of fluvial deposits.

7.2. Utility of Topographic Metrics of Erosion and Divide Mobility

Because drainage area change immediately affects the spatial pattern of the channel steepness index, it is tempting to conclude that k_{sn} is a flawed metric of landscape evolution. However, in all models considered, the relationship between k_{sn} and erosion rate does not change as a consequence of a change in drainage area. Indeed, the relationship between k_{sn} and erosion rate is central to the conceptual model presented in

Figure 2 and the competing positive and negative feedbacks considered in our analysis. As in all departures from steady state conditions, however, the relationship between k_{sn} and erosion rate can be complicated by adjustments in sediment flux relative to sediment transport capacity, in the degree of alluvial cover blanketing channel bed and banks, and channel width [e.g., *Sklar and Dietrich*, 2004, 2006; *Finnegan et al*., 2007; *Gasparini et al*., 2007; *Lague*, 2010; *Yanites et al*., 2011; *DiBiase et al*., 2015], factors that must be considered in interpretation of natural landscapes.

Fundamentally, divide migration may complicate the relationship between rock uplift rate and erosion rate, but not the interpretation of k_{sn} as a metric of erosion rates. As illustrated in Figure 2, this central tenet permits a general understanding of the style and proximal causes of landscape evolution following a change in drainage area. A gain or loss of drainage area affects the erosive power of a stream but involves no immediate change to the river profile—elevation and gradient are unchanged at the moment of area change. However, the spatial pattern of river slope relative to drainage area (the channel steepness) and thus erosion rate does change at the moment of loss or addition of drainage area, as effectively illustrated in χ-transformed river profiles (e.g., Figures 2 and 4).

Under conditions of spatially uniform rock uplift rate, U, and erodibility, K, maps of cross-divide χ anomalies can be effective in identifying potentially unstable or actively mobile drainage divides [*Willett et al*., 2014]. However, there are many circumstances where χ anomalies can be sustained across stable divides (e.g., Figures 3, 6a, and 10e) and thus are easily confounded as a metric of divide mobility. Although all metrics of divide mobility will face challenges in applications in natural landscapes, we demonstrate that several alternative potential divide mobility metrics are more reliable and perform well in model simulations (Figure 10) and in the Taiwan example examined (Figure 12). Importantly the metrics we explore are all directly tied to the root cause of divide mobility—a difference in erosion rate on either side of a divide [e.g., *Gilbert*, 1877]—and do not rest on a set of restrictive assumptions about downstream conditions like the χ-anomaly metric.

8. Conclusions

Both 1-D and 2-D numerical simulations illustrate that in many circumstances perturbations to a landscape resulting in drainage divide migration or drainage area capture do not lead to a positive feedback mechanism inducing further divide migration or capture. The perturbation of channel steepness patterns, and thus the pattern of erosion rates resulting from drainage area change, immediately triggers a pattern of differential erosion that acts as a negative feedback, driving river profiles back toward equilibrium. Modeling results illustrate only minor deviations from steady state channel profile forms during periods of active, progressive, headward divide migration in areas of active rock uplift (e.g., as shown in Figure 6), implying that the negative feedback of river profile response to drainage area change dominates landform evolution in these settings. Detectable and interpretable perturbation of river profiles attributable to drainage area change is restricted to periods following large (>5% total drainage area) discrete river capture events and circumstances in which catchments are encroached from all sides (e.g., Figure 9 and Movie S3). Large perturbations following significant stream capture events will persist longer in settings where the erosional efficiency of rivers (largely set by rock properties and the erosivity of the climate) is low.

We introduce a nondimensional divide migration number, N_{Dm}, that is defined as the ratio of the timescale of channel response to a change in drainage area to the timescale of divide migration, T_{dA}/T_{Dm}, to assess the strength of the positive and negative divide migration feedback mechanisms. For headward divide migration in tectonically active settings, the timescale of channel profile response to a change in drainage area is always more than an order of magnitude shorter than the timescale of divide migration driven by tectonic (or climatic) perturbation, explaining the maintenance of quasi-steady river profile forms during periods of active divide migration in our simulations. We show that the divide migration number in this scenario is invariant with changes in U, K, or channel length, L, and is always much less than unity. Conversely, where divide migration is triggered perpendicular to the topographic grain, isolated catchments encroached from all sides can develop, allowing the positive area loss feedback to locally keep pace with channel profile response, as has been discussed by *Goren et al*. [2014], *Willett et al*. [2014], and *Yang et al*. [2015], here sustaining conditions near $N_{Dm} = 1$.

Because channel profiles maintain a quasi-steady form during active headward divide migration and the fact that cross-divide differences in χ can arise for many reasons unrelated to divide mobility, we propose more

robust metrics of divide mobility than cross-divide χ differences. In both numerical landscapes and a natural example in Taiwan, cross-divide differences in mean headwater hillslope gradient, mean headwater local relief (500 m radius), and channel bed elevation at a reference drainage area (e.g., 0.1–1 km^2) are all more faithful metrics of the direction and rate of divide mobility than cross-divide differences in χ or χ-transformed river profile forms. Cross-divide differences in mean headwater local relief are likely to be the most robust metric of divide mobility given the potential for threshold hillslope gradients and differences in fluvial channel head locations.

Our analysis shows that river profiles in tectonically active settings are generally best interpreted in terms of spatiotemporal patterns in rock uplift rate relative to baselevel, climate, or rock properties and not in terms of changes in drainage area associated with divide migration and network reorganization. However, large stream capture events that have occurred more recently than the timescale of channel profile response will of course leave a clear signature in channel profiles, and this possibility should be considered in efforts to extract information about the spatial pattern or history of climate or tectonics from modern topography.

Acknowledgments

Data supporting our conclusions can be found in Table 1, Figure captions, supporting information, or in publically accessible digital topographic models (http://earthexplorer.usgs.gov/). A.M.F.'s contribution was supported by EAR-1450970 and W.B.O.'s contribution by EAR-1220453. The authors declare no conflicting financial interests. We thank S. Mudd, F. Pazzaglia, M. Attal, and J. Buffington for insightful critical reviews that notably improved the manuscript and S. Willett and J. Braun for helpful, clarifying, and motivating discussions. We also thank S. Willett for sharing animations of DAC simulations of divide migration analogous to our numerical experiments.

References

Attal, M., P. Cowie, A. Whittaker, D. Hobley, G. Tucker, and G. Roberts (2011), Testing fluvial erosion models using the transient response of bedrock rivers to tectonic forcing in the Apennines, Italy, *J. Geophys. Res.*, *116*, F02005, doi:10.1029/2010JF001875.

Bishop, P. (1995), Drainage rearrangement by river capture, beheading and diversion, *Prog. Phys. Geogr.*, *19*(4), 449–473, doi:10.1177/030913339501900402.

Bonnet, S. (2009), Shrinking and splitting of drainage basins in orogenic landscapes from the migration of the main drainage divide (vol 2, pg 766, 2009), *Nat. Geosci.*, *2*(12), 897–897, doi:10.1038/ngeo700.

Braun, J., and S. D. Willett (2013), A very efficient O(n), implicit and parallel method to solve the stream power equation governing fluvial incision and landscape evolution, *Geomorphology*, *180*, 170–179, doi:10.1016/j.geomorph.2012.10.008.

Brocard, G., et al. (2012), Rate and processes of river network rearrangement during incipient faulting: The case of the Cahabón River, Guatemala, *Am. J. Sci.*, *312*(5), 449–507, doi:10.2475/05.2012.01.

Castelltort, S., L. Goren, S. D. Willett, J. D. Champagnac, F. Herman, and J. Braun (2012), River drainage patterns in the New Zealand Alps primarily controlled by plate tectonic strain, *Nat. Geosci.*, *5*(10), 744–748, doi:10.1038/ngeo1582.

Clark, M. K., L. M. Schoenbohm, L. H. Royden, K. X. Whipple, B. C. Burchfiel, X. Zhang, W. Tang, E. Wang, and L. Chen (2004), Surface uplift, tectonics, and erosion of eastern Tibet from large-scale drainage patterns, *Tectonics*, *23*, TC1006, doi:10.1029/2002TC001402.

Clark, M. K., J. S. Maheo, and K. A. Farley (2005), The non-equilibrium landscape of the southern Sierra Nevada, California, *GSA Today*, *15*(9), 4–10, doi:10.1130/1052-5173(2005)015<4:TNELOT>2.0.CO;2.

Clubb, F. J., S. M. Mudd, D. T. Milodowski, M. D. Hurst, and L. J. Slater (2014), Objective extraction of channel heads from high-resolution topographic data, *Water Resour. Res.*, *50*, 4283–4304, doi:10.1002/2013WR015167.

Craddock, W. H., D. W. Burbank, B. Bookhagen, and E. J. Gabet (2007), Bedrock channel geometry along an orographic rainfall gradient in the upper Marsyandi River valley in central Nepal, *J. Geophys. Res.*, *112*, F03007, doi:10.1029/2006JF000589.

Cyr, A. J., D. E. Granger, V. Olivetti, and P. Molin (2010), Quantifying rock uplift rates using channel steepness and cosmogenic nuclide-determined erosion rates: Examples from northern and southern Italy, *Lithosphere*, *2*(3), 188–198, doi:10.1130/l96.1.

Davis, W. M. (1903), The stream contest along the Blue Ridge, *Bull. Geogr. Soc. Phila.*, *3*(5), 213–244.

DiBiase, R. A., and K. X. Whipple (2011), The influence of erosion thresholds and runoff variability on the relationships among topography, climate, and erosion rate, *J. Geophys. Res.*, *116*, F04036, doi:10.1029/2011JF002095.

DiBiase, R. A., K. X. Whipple, A. M. Heimsath, and W. B. Ouimet (2010), Landscape form and millennial erosion rates in the San Gabriel Mountains, CA, *Earth Planet. Sci. Lett.*, *289*(1-2), 134–144, doi:10.1016/j.epsl.2009.10.036.

DiBiase, R. A., A. M. Heimsath, and K. X. Whipple (2012), Hillslope response to tectonic forcing in threshold landscapes, *Earth Surf. Processes Landforms*, *37*(8), 855–865, doi:10.1002/esp.3205.

DiBiase, R. A., K. X. Whipple, M. P. Lamb, and A. M. Heimsath (2015), The role of waterfalls and knickzones in controlling the style and pace of landscape adjustment in the western San Gabriel Mountains, California, *Geol. Soc. Am. Bull.*, *127*(3-4), 539–559, doi:10.1130/b31113.1.

Duvall, A., E. Kirby, and D. W. Burbank (2004), Tectonic and lithologic controls on bedrock channel profiles and processes in coastal California, *J. Geophys. Res.*, *109*, F03002, doi:10.1029/2003JF000086.

Finnegan, N. J., L. S. Sklar, and T. K. Fuller (2007), Interplay of sediment supply, river incision, and channel morphology revealed by the transient evolution of an experimental bedrock channel, *J. Geophys. Res.*, *112*, F03S11, doi:10.1029/2006JF000569.

Gasparini, N. M., K. X. Whipple, and R. L. Bras (2007), Predictions of steady state and transient landscape morphology using sediment-flux-dependent river incision models, *J. Geophys. Res.*, *112*, F03S09, doi:10.1029/2006JF000567.

Giachetta, E., A. Refice, D. Capolongo, N. M. Gasparini, and F. J. Pazzaglia (2014), Orogen-scale drainage network evolution and response to erodibility changes: Insights from numerical experiments, *Earth Surf. Processes Landforms*, *39*(9), 1259–1268, doi:10.1002/esp.3579.

Gilbert, G. K. (1877), Report on the Geology of the Henry Mountains (Utah), *Survey of the Rocky Mountains Region Rep.*, United States Geological Survey, Washington, D.C.

Glock, W. S. (1931), The development of drainage systems: A synoptic view, *Geogr. Rev.*, *21*(3), 475–482, doi:10.2307/209434.

Godard, V., D. L. Bourles, F. Spinabella, D. W. Burbank, B. Bookhagen, G. B. Fisher, A. Moulin, and L. Leanni (2014), Dominance of tectonics over climate in Himalayan denudation, *Geology*, *42*(3), 243–246, doi:10.1130/g35342.1.

Goren, L., S. D. Willett, F. Herman, and J. Braun (2014), Coupled numerical-analytical approach to landscape evolution modeling, *Earth Surf. Processes Landforms*, *39*(4), 522–545, doi:10.1002/esp.3514.

Hack, J. T. (1957), Studies of longitudinal stream profiles in Virginia and Maryland, *U.S. Geological Survey Professional Paper*, *294-B*, 97.

Harkins, N., E. Kirby, A. Heimsath, R. Robinson, and U. Reiser (2007), Transient fluvial incision in the headwaters of the Yellow River, northeastern Tibet, China, *J. Geophys. Res.*, *112*, F03S04, doi:10.1029/2006JF000570.

Hasbargen, L. E., and C. Paola (2000), Landscape instability in an experimental drainage basin, *Geology*, *28*(12), 1067–1070, doi:10.1130/0091-7613(2000)28<1067:liiaed>2.0.co;2.

Hilley, G. E., and J. R. Arrowsmith (2008), Geomorphic response to uplift along the Dragon's Back pressure ridge, Carrizo Plain, California, *Geology*, *36*(5), 367–370, doi:10.1130/G24517A.1.
Howard, A. D. (1994), A detachment-limited model of drainage basin evolution, *Water Resour. Res.*, *30*, 2261–2285, doi:10.1029/94WR00757.
Kirby, E., and W. Ouimet (2011), Tectonic geomorphology along the eastern margin of Tibet: Insights into the pattern and processes of active deformation adjacent to the Sichuan Basin, *Geol. Soc., Lond., Spec. Publ.*, *353*, 165–188, doi:10.1144/SP353.9.
Kirby, E., and K. Whipple (2001), Quantifying differential rock-uplift rates via stream profile analysis, *Geology*, *29*, 415–418, doi:10.1130/0091-7613(2001)029<0415:QDRURV>2.0.CO;2.
Kirby, E., and K. X. Whipple (2012), Expression of active tectonics in erosional landscapes, *J. Struct. Geol.*, *44*, 54–75, doi:10.1016/j.jsg.2012.07.009.
Lague, D. (2010), Reduction of long-term bedrock incision efficiency by short-term alluvial cover intermittency, *J. Geophys. Res.*, *115*, F02011, doi:10.1029/2008JF001210.
Lague, D. (2014), The stream power river incision model: Evidence, theory and beyond, *Earth Surf. Processes Landforms*, *39*(1), 38–61, doi:10.1002/esp.3462.
Lague, D., N. Hovius, and P. Davy (2005), Discharge, discharge variability, and the bedrock channel profile, *J. Geophys. Res.*, *110*, F04006, doi:10.1029/2004JF000259.
Lavé, J., and J.-P. Avouac (2001), Fluvial incision and tectonic uplift across the Himalayas of central Nepal, *J. Geophys. Res.*, *106*, 26,561–526,591, doi:10.1029/2001JB000359.
Miller, S. R., S. L. Baldwin, and P. G. Fitzgerald (2012), Transient fluvial incision and active surface uplift in the Woodlark Rift of eastern Papua New Guinea, *Lithosphere*, *4*(2), 131–149, doi:10.1130/l135.1.
Miller, S. R., P. B. Sak, E. Kirby, and P. R. Bierman (2013), Neogene rejuvenation of central Appalachian topography: Evidence for differential rock uplift from stream profiles and erosion rates, *Earth Planet. Sci. Lett.*, *369*, 1–12, doi:10.1016/j.epsl.2013.04.007.
Montgomery, D. R., and E. Foufoula-Georgiou (1993), Channel network source representation using digital elevation models, *Water Resour. Res.*, *29*, 3925–3934, doi:10.1029/93WR02463.
Mudd, S. M., M. Attal, D. T. Milodowski, S. W. D. Grieve, and D. A. Valters (2014), A statistical framework to quantify spatial variation in channel gradients using the integral method of channel profile analysis, *J. Geophys. Res. Earth Surf.*, *119*, 138–152, doi:10.1002/2013JF002981.
Ouimet, W. B., K. X. Whipple, and D. E. Granger (2009), Beyond threshold hillslopes: Channel adjustment to base-level fall in tectonically active mountain ranges, *Geology*, *37*(7), 579–582, doi:10.1130/G30013A.1.
Passalacqua, P., T. Do Trung, E. Foufoula-Georgiou, G. Sapiro, and W. E. Dietrich (2010), A geometric framework for channel network extraction from lidar: Nonlinear diffusion and geodesic paths, *J. Geophys. Res.*, *115*, F01002, doi:10.1029/2009JF001254.
Pelletier, J. D. (2004), Persistent drainage migration in a numerical landscape evolution model, *Geophys. Res. Lett.*, *31*, L20501, doi:10.1029/2004GL020802.
Perron, J. T., and L. Royden (2012), An integral approach to bedrock river profile analysis, *Earth Surf. Processes Landforms*, *38*(6), 570–576, doi:10.1002/esp.3302.
Prince, P. S., J. A. Spotila, and W. S. Henika (2010), New physical evidence of the role of stream capture in active retreat of the Blue Ridge escarpment, southern Appalachians, *Geomorphology*, *123*(3-4), 305–319, doi:10.1016/j.geomorph.2010.07.023.
Prince, P. S., J. A. Spotila, and W. S. Henika (2011), Stream capture as driver of transient landscape evolution in a tectonically quiescent setting, *Geology*, *39*(9), 823–826, doi:10.1130/g32008.1.
Scherler, D., B. Bookhagen, and M. R. Strecker (2014), Tectonic control on Be-10-derived erosion rates in the Garhwal Himalaya, India, *J. Geophys. Res. Earth Surf.*, *119*, 83–105, doi:10.1002/2013JF002955.
Sklar, L. S., and W. E. Dietrich (2004), A mechanistic model for river incision into bedrock by saltating bed load, *Water Resour. Res.*, *40*, W06301, doi:10.1029/2003WR002496.
Sklar, L. S., and W. E. Dietrich (2006), The role of sediment in controlling steady-state bedrock channel slope: Implications of the saltation-abrasion incision model, *Geomorphology*, *82*(1-2), 58–83, doi:10.1016/j.geomorph.2005.08.019.
Stark, C. P. (2010), Oscillatory motion of drainage divides, *Geophys. Res. Lett.*, *37*, L04401, doi:10.1029/2009GL040851.
Stock, J. D., and D. R. Montgomery (1999), Geologic constraints on bedrock river incision using the stream power law, *J. Geophys. Res.*, *104*, 4983–4993, doi:10.1029/98JB02139.
Tucker, G. E. (2004), Drainage basin sensitivity to tectonic and climatic forcing: Implications of a stochastic model for the role of entrainment and erosion thresholds, *Earth Surf. Process. Landforms*, *29*, 185–205, doi:10.1002/esp.1020.
Tucker, G. E., and G. R. Hancock (2010), Modelling landscape evolution, *Earth Surf. Processes Landforms*, *35*(1), 28–50, doi:10.1002/esp.1952.
Tucker, G. E., and K. X. Whipple (2002), Topographic outcomes predicted by stream erosion models: Sensitivity analysis and intermodel comparison, *J. Geophys. Res.*, *107*(B9), 2179, doi:10.1029/2001JB000162.
Tucker, G. E., S. Lancaster, N. M. Gasparini, and R. Bras (2001), The channel-hillslope integrated landscape development model (CHILD), in *Landscape Erosion and Evolution Modeling*, edited by S. Harmon and W. W. Doe III, pp. 349–388, Springer, doi:10.1007/978-1-4615-0575-4_12.
Whipple, K. X. (2001), Fluvial landscape response time: How plausible is steady state denudation?, *Am. J. Sci.*, *301*, 313–325, doi:10.2475/ajs.301.4-5.313.
Whipple, K. X., and G. E. Tucker (1999), Dynamics of the stream-power river incision model: Implications for height limits of mountain ranges, landscape response timescales, and research needs, *J. Geophys. Res.*, *104*, 17,661–17,674, doi:10.1029/1999JB900120.
Whipple, K. X., R. A. DiBiase, and B. Crosby (2013), Bedrock rivers, in *Treatise on Fluvial Geomorphology*, edited by J. J. Shroder and E. Wohl, vol. 9 pp. 550–573, Academic Press, San Diego, Calif., doi:10.1016/B978-0-12-374739-6.00254-2.
Whipple, K. X., R. A. DiBiase, W. B. Ouimet, and A. M. Forte (2017), Preservation or piracy: Diagnosing low-relief, high-elevation surface formation mechanisms, *Geology*, doi:10.1130/G38490.1.
Whittaker, A. C. (2012), How do landscapes record tectonics and climate?, *Lithosphere*, *4*(2), 160–164, doi:10.1130/rf.l003.1.
Whittaker, A. C., P. A. Cowie, M. Attal, G. E. Tucker, and G. P. Roberts (2007), Bedrock channel adjustment to tectonic forcing: Implications for predicting river incision rates, *Geology*, *35*(2), 103–106, doi:10.1130/g20738.1.
Willett, S. D., S. W. McCoy, J. T. Perron, L. Goren, and C. Y. Chen (2014), Dynamic reorganization of river basins, *Science*, *343*(6175), doi:10.1126/science.1248765.
Wobus, C., K. X. Whipple, E. Kirby, N. Snyder, J. Johnson, K. Spyropolou, B. Crosby, and D. Sheehan (2006), Tectonics from topography: Procedures, promise, and pitfalls, *Geol. Soc. Am. Spec. Pap.*, *398*, 55–74, doi:10.1130/2006.2398(04).
Yang, R., S. D. Willett, and L. Goren (2015), In situ low-relief landscape formation as a result of river network disruption, *Nature*, *520*(7548), 526–529, doi:10.1038/nature14354.

Yanites, B. J., G. E. Tucker, H. Hsu, C. Chen, Y. Chen, and K. J. Mueller (2011), The influence of sediment cover variability on long-term river incision rates: An example from the Peikang River, central Taiwan, *J. Geophys. Res.*, *116*, F03016, doi:10.1029/2010JF001933.

Yanites, B. J., T. A. Ehlers, J. K. Becker, M. Schnellmann, and S. Heuberger (2013), High magnitude and rapid incision from river capture: Rhine River, Switzerland, *J. Geophys. Res. Earth Surf.*, *118*, 1060–1084, doi:10.1002/jgrf.20056.